Nanoscale

ROYAL SOCIETY OF CHEMISTRY

REVIEW

View Article Online
View Journal | View Issue

Cite this: *Nanoscale*, 2025, **17**, 1790

Advancements in framework materials for enhanced energy harvesting

Anulipsa Priyadarshini,†[a] S. Divya, †[b] Jaykishon Swain,[a] Niharika Das,[a] Subrat Swain,[a] Sugato Hajra, *[c] Swati Panda,[c] Raghabendra Samantaray,[a] Mohamed Belal,[c] Kushal Ruthvik Kaja,[c] Naveen Kumar,[d] Hoe Joon Kim, [c] Tae Hwan Oh, [b] Venkateswaran Vivekananthan[e,f] and Rojalin Sahu *[a]

Energy harvesting, the process of capturing ambient energy from various sources and converting it into usable electrical power, has attracted a lot of attention due to its potential to provide long-term and self-sufficient energy solutions. This comprehensive review thoroughly explores the use of metal–organic frameworks (MOFs) and covalent organic frameworks (COFs) for energy harvesting by piezoelectric and triboelectric nanogenerators (PENGs and TENGs). It begins by classifying and outlining the structural diversity of MOFs and COFs, which is key to understanding their importance in energy applications. Key characterization techniques are focused on emphasizing their importance in optimizing material properties for efficient energy conversion. The working mechanisms of PENGs and TENGs are discussed, focusing on their ability to transform mechanical energy into electrical energy and their advantages in operation. The use of MOFs and COFs in energy harvesting applications is then discussed, including synthesis procedures, unique characteristics relevant to electricity conversion, and various practical applications such as self-powered sensors and wearable electronics. Current challenges such as stability, scalability, and performance improvements are explored, as well as proposed future improvements to help advance current research. Finally, the study highlights the importance of framework materials for the development of energy harvesting systems, providing an invaluable resource for academics and engineers seeking to exploit the potential of these materials for renewable energy sources. The goal of this article is to stimulate further invention and implementation of efficient materials-based energy harvesting framework devices by integrating recent advances and mapping future possibilities.

Received 1st November 2024,
Accepted 22nd November 2024

DOI: 10.1039/d4nr04570j

rsc.li/nanoscale

1. Introduction

A piezoelectric nanogenerator (PENG) uses the piezoelectric effect to transform mechanical energy into electrical energy, making use of materials generating electric charges when mechanically stressed.[1,2] PENGs are small, efficient devices that can power small electronics and sensors indefinitely, making them perfect for use in wearable technology, wireless sensors, and self-powered systems.[3–5] The triboelectric nanogenerator (TENG) represents a groundbreaking advancement in energy harvesting, offering a novel and sustainable solution for converting mechanical energy into electrical energy. This innovative technology harnesses the principles of contact electrification and electrostatic induction, where materials accumulate electrical charge through friction.[6,7] The significance of TENGs extends far beyond their simple and cost-effective design; they play a pivotal role in addressing environmental concerns. By effectively capturing energy from everyday actions and natural phenomena, TENGs reduce our reliance on traditional power sources that contribute to environmental degradation. This not only promotes a cleaner, more sustainable energy landscape but also opens new avenues for powering low-energy devices and sensors, contributing to a greener and more efficient use of resources.[8–10] The advent of TENG technology marks a crucial step towards harmonizing our

[a]*Future Materials Laboratory, School of Applied Sciences, Kalinga Institute of Industrial Technology (KIIT), Deemed to be University, Bhubaneswar, 751024, India. E-mail: rsahufch@kiit.ac.in*
[b]*Department of School of Chemical Engineering, Yeungnam University, Gyeongsan, 712–749, Republic of Korea*
[c]*Department of Robotics and Mechatronics Engineering, Daegu Gyeongbuk Institute of Science and Technology, Daegu, 42988, South Korea. E-mail: sugatohajra@dgist.ac.kr*
[d]*Department Materials Engineering, Indian Institute of Science, CV Raman Avenue, Bangalore, 560012, India*
[e]*Center for Flexible Electronics, Department of Electronics and Communication Engineering, Koneru Lakshmaiah Education Foundation, Guntur 522502, India*
[f]*Department of Integrated Research and Discovery, Koneru Lakshmaiah Education Foundation, Guntur 522502, India*
†These authors have equal contributions.

energy needs with the pressing demands of environmental stewardship.

The word "reticular" originates from the Latin term "rēticulum" which means "netlike". Reticular Chemistry focuses on the precise control of bond formation and cleavage within molecules.[11] Metal organic frameworks (MOFs) are crystalline solids crafted through reticular chemistry, establishing directional chemical bonds for stable extended structures.[12] Further, in addition to MOFs, covalent organic frameworks (COFs), and zeolitic imidazolate frameworks (ZIFs), marked a significant advancement in both coordination chemistry and materials science. Reticular chemistry played a pivotal role in extending the scope of organic chemistry beyond molecules and polymers.[13] By employing reticular chemistry, organic building blocks were linked to form crystalline two- and three-dimensional frameworks, offering innovative tools for material design in both MOFs and COFs.[13,14] MOFs are formed through the coordination assembly between metal ions and organic ligands.[4,5] This impeccable framework was initially witnessed and built by Yaghi *et al.* in 1995.[15] ZIFs, a subclass of MOFs, are analogous to zeolites and usually formed by metal ions and imidazole-based ligands. The development of porous ZIFs featuring characteristics of both zeolites and MOFs, combining uniform cage-like pores with high crystallinity and permanent porosity, initiated intense research in this field.[16]

COFs, another class of crystalline porous framework material, represent a distinct category created by connecting organic units through covalent bonds involving lighter elements like H, B, C, N, O, and Si. As the pioneering class of both two-dimensional and three-dimensional crystalline organic solids, COFs are characterized by their molecular structures arranged in repeating patterns, bonded covalently.[17] In 2005, Omar M. Yaghi and his coworkers introduced the first crystalline extended organic frameworks, COF-1 and COF-5, demonstrating the reversible nature of boroxine and boronate ester formations, respectively.[18] Notably the porosity of framework materials is intimately connected to their unique structural composition, forming highly ordered, lattice-like frameworks. This, coupled with the ability to modify the chemical properties of pore surfaces and positions. The precise control over their porosity allows for the engineering of MOFs, COFs and ZIFs for various applications like energy storage applications such as batteries,[19,20] supercapacitors,[21–25] pseudo capacitors,[26–28] fuel cells,[29–32] electrochemical conversions,[33–35] drug delivery,[36–39] sensing,[40–43] gas adsorption,[44–47] and separations,[48–51] as well as providing numerous active sites for catalytic reactions.[52–54] With their tailor-made morphology, high surface area, and tunable pore dimensions, MOFs can be used to harvest energy through various applications like hydrogen storage[55–57] and fabrications of TENG devices.[58,59]

This review study focuses on the application of MOFs and COFs in energy harvesting, specifically through PENGs and TENGs. MOFs and COFs have different structural characteristics and surface chemistry, making them ideal options for energy conversion applications. Understanding their structural diversity and the methodologies used to characterize these materials is critical to improving their performance in energy harvesting systems. This review article presents a detailed analysis of these topics and clarify the working mechanisms of PENG and TENG. The use of MOFs and COFs in energy harvesting applications is then discussed, including synthesis procedures, characteristics related to energy conversion, and various practical applications such as self-powered sensors and wearable electronics. Current challenges and future approaches to improve the performance of MOF and COF systems based on energy harvesting are carefully explored. In conclusion, the summary highlights important findings and highlights the importance of this study in consolidating current advances and guiding future research efforts in the rapidly growing field of materials-based energy harvesting framework technologies. This review summarizes the current information which is crucial for using MOFs and COFs for various energy harvesting applications. The research not only identifies current obstacles but also suggests future improvements to accelerate the development and implementation of efficient energy harvesting devices based on framework materials critical for researchers and industry workers.

2. Classification of framework material

There are various ways to classify the framework materials as shown in Fig. 1. But here we have mainly focussed based on their structure and properties such as coordination frameworks which include MOFs, ZIFs (the analogous of zeolites), and COFs. MOFs are a class of materials consisting of metal ions or clusters coordinated with organic linkers to form 1D, 2D, and 3D structures.[60,61] They are also known as porous coordination polymers due to their porosity. These materials exhibit remarkable structural and chemical tunability, allowing for customization of their properties such as stability, porosity, and particle morphology.[14,62–64] The structure and properties of MOFs can be classified based on the metal nodes and organic linkers present within the crystal, and their confirmation and stabilization can be achieved using various techniques. MOFs are crystalline and microporous materials that have various types and structures. These structures typically exhibit a porosity that exceeds 50% of the total volume of the MOF crystal.[65] The construction of these structures is achieved through various assembly techniques, ranging from weaker π–π stacking interactions to stronger forces like covalent bonding.[66–70] The 2D-MOFs and 2D-COFs can take the advantage of the strong π–π interactions and redox processes to enhance the electric conductivity while activating the unique electrocatalytic properties of aromatic N4-macrocycle.[71] MOFs can also be classified based on their connectivity, such as (3,6)- and (3,5)-connected nets. ZJNU-16 and ZJNU-17 are two MOFs that differ in structure and properties. ZJNU-16 is a (3,6)-connected network with a trinuclear Co3-based cluster as an inorganic SBU, while ZJNU-17 is a (3,5)-connected frame-

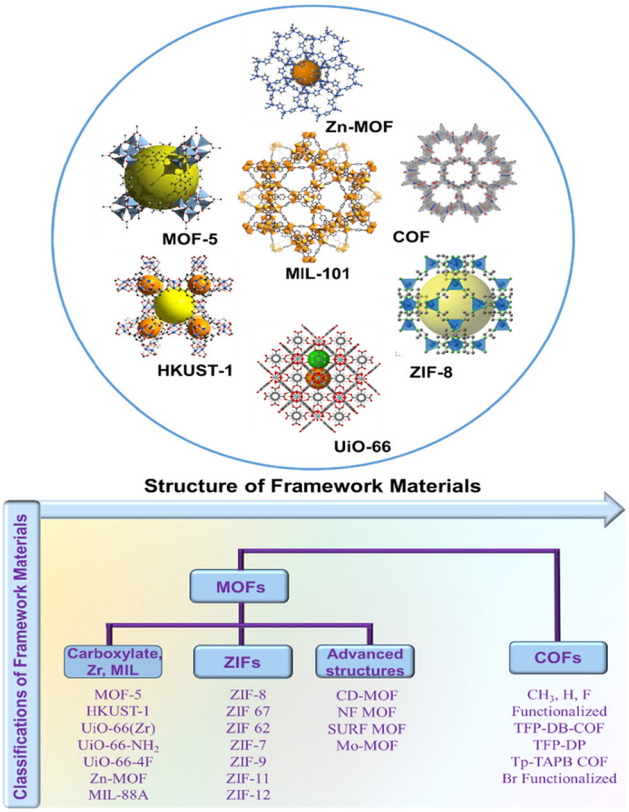

Fig. 1 Structure of various framework materials and their classifications.

work with a nanotubular helical Co-carboxylate chain as an inorganic SBU.[72] The different ligand configurations in MOFs can lead to distinct architectures and functionalities.[73]

ZIFs are the tetrahedral structured subclass of MOFs, formed by linking tetrahedral nodes with building units, with an angle close to that of the ∠(Si–O–Si) = 145° as found in zeolites.[74] The framework structure is composed of metal ions or clusters connected by imidazole linkers result in high chemical, thermal, mechanical as well as architectural stability with ∠(M–imidazolate–M) angle.[74] The basic structure of ZIFs can be depicted as follows: $[M(Im)_2]_n$. Where M represents the metal ion or cluster (*e.g.*, Zn, Co, Cu) and Im represents the imidazolate linker. The value of n indicates the stoichiometry of the framework.[75] For example, in ZIF-8, which is one of the most well-known ZIFs, the structure consists of Zn^{2+} ions connected by 2-methylimidazolate (2-MeIm) ligands. The chemical structure of ZIF-8 can be represented as: $[Zn(2\text{-MeIm})_2]_n$.[76] This structural classification making ZIFs as a promising material for various applications such as gas storage and separation, catalysis, drug delivery, and sensing.[77–81] Additionally, their facile synthesis and functionalization further enhance their versatility and potential in addressing contemporary challenges in energy, environmental, and biomedical fields. Numerous research articles have extensively explored the synthesis methods, characterization techniques, and applications of ZIFs, highlighting their promising role as multifunctional materials with tailored properties for specific applications.

By functionalizing framework materials, their performance in TENGs can be tuned and amplified, contributing to higher power output, and advancing sustainable energy solutions. Additionally, 2D-MOFs and 2D-COFs exhibit promise in renewable energy systems like supercapacitors and metal–air batteries due to their high surface area and organized porous structures.[82] For instance, ZIF-67, a type of MOF, has demonstrated high output performance in self-powered TENG devices.[83] Combining MOFs with MXenes has led to the development of composites for TENGs as self-powered flexible sensors,[84] electrochemical energy storage and conversion systems, including supercapacitors and lithium-ion batteries.[85] Synthesizing bimetallic MOFs like ZIF-8@ZIF-67 has resulted in electrode materials for supercapacitors with high specific capacitance and extended cycle life.[86] MOF-5 has been used as a tribo-layer in TENG devices, demonstrating its potential for energy harvesting from mechanical motion. The use of conductive polymers, such as polyaniline, in combination with framework materials has also been explored for TENG applications. These hybrid materials have shown enhanced electrical conductivity and improved performance in energy harvesting.[59] These examples underscore the potential of framework materials in diverse energy harvest applications, benefiting from precise control over their porosity. Overall, MOFs offer promising opportunities for energy harvesting in various fields.

3. Characterisation and synthesis process of framework materials

Characterization of framework materials such as MOFs, COFs, and ZIFs involves a range of techniques to assess their structural, chemical, and physical properties. One of the fundamental techniques used is powder X-ray diffraction (PXRD), which is employed to determine the crystallinity of these materials. PXRD involves directing X-rays at a powdered sample and analysing the diffraction pattern produced. The resulting diffraction pattern provides information about the arrangement of atoms or molecules within the framework, helping to identify the crystal structure and confirm the presence of specific phases. In addition to PXRD, other techniques like scanning electron microscopy (SEM) and transmission electron microscopy (TEM), Fourier transform infrared spectroscopy (FTIR), nuclear magnetic resonance (NMR) spectroscopy, thermogravimetric analysis (TGA), BET (Brunauer–Emmett–Teller), X-ray photoelectron spectroscopy (XPS) commonly used for characterizing framework materials. SEM and TEM are used to visualize the morphology and internal structure of framework materials at the micro- and nanoscale, respectively. These techniques provide information about particle size, shape, porosity, and surface features. FTIR is employed to analyse the functional groups present in framework materials. It provides information about chemical bonding, coordination

modes, and potential interactions within the framework structure. NMR spectroscopy, including solid-state NMR, can be used to study the local environment of nuclei within the framework, offering insights into chemical connectivity, guest–host interactions, and dynamic behaviour. TGA is utilized to investigate the thermal stability and decomposition behaviour of framework materials under controlled temperature conditions. This information is crucial for assessing their suitability for specific applications, especially those involving high temperatures. Gas adsorption and desorption analysis were characterised using gas sorption techniques such as BET to determine the surface area, pore size distribution, and gas adsorption capacities of framework materials, which are essential for applications like gas storage and separation. XPS provides elemental composition and chemical state information of the surface layers of framework materials, aiding in understanding surface functionalities, defects, and electronic properties.

For energy applications like TENG, two key techniques used to study the surface property and mechanical behaviour of the materials are Kelvin probe force microscopy (KPFM) and atomic force microscopy (AFM). KPFM and AFM are complementary techniques that offer detailed insights into the electrical, mechanical, and surface properties of triboelectric nanogenerators. KPFM is a powerful technique that combines atomic force microscopy (AFM) with Kelvin probe measurements. It is used to map the surface potential and work function of materials at the nanoscale. In the context of TENGs, KPFM can provide insights into the surface charge distribution, contact potential difference, and charge transfer mechanisms during triboelectric interactions. By analysing the KPFM images and data, researchers can evaluate the electrical properties of TENG surfaces, assess charge generation and dissipation, and optimize the device design for enhanced performance. AFM is a versatile imaging technique that allows for high-resolution imaging of surfaces and measurement of mechanical properties at the nanoscale. For TENG characterization, AFM can be used to visualize surface topography, measure surface roughness, and investigate material properties such as stiffness, elasticity, and adhesion. AFM-based techniques like dynamic mode AFM and contact mode AFM can provide valuable information about the morphology and mechanical behaviour of TENG components, including the triboelectric layers, electrodes, and interface regions. These insights are essential for understanding the structural integrity, durability, and frictional properties of TENGs, ultimately guiding the optimization of their performance for energy harvesting applications. By employing these characterization methods, researchers can comprehensively evaluate the properties and performance of framework materials, guiding their design, synthesis, and application in various fields ranging from catalysis and sensing to energy storage and can advance the development of efficient and robust TENG devices for energy harvesting. Some of the common techniques of synthesis or processing of frame work materials for energy harvesting includes: hydrothermal synthesis, microwave-assisted synthesis, sonochemical synthesis, electrochemical synthesis, and electrospinning techniques. In hydrothermal synthesis of framework materials involves dissolving metal salts and organic linkers in a solvent followed by heating in a sealed vessel. It allows slow crystallization of MOFs and COFs under controlled temperature and pressure, yielding high crystallinity for high performance of energy harvesters.[87,88] The microwave assisted synthesis method generally a microwave radiation is utilized to provide homogeneous heating, which speeds up the crystallization process and cuts down reaction time from hours to minutes.[89,90] It creates MOFs and COFs with uniform particle sizes and good crystallinity, which are perfect for scaling up with better control over product morphology. Using ultrasonic waves, the sonochemical method creates microbubbles in the reaction mixture, enhancing mass transfer and accelerating nucleation.[91] It allows MOF, COF, and composite synthesis with fine control over particle size and morphology, making it beneficial for producing nanostructured materials and composites with unique properties for high performance energy devices. Metal ions are generated *in situ* by electrochemical dissolution, eliminating the need for external metal salts in case of electrochemical synthesis of framework material. This technique offers precise control over metal ion concentration and reduces by-products. It is advantageous for MOF and MOF-polymer composite production, allowing deposition on conductive substrates for device applications.[92,93] Electrospinning method basically uses a polymer solution containing dispersed MOF or COF precursors is subjected to a high-voltage electric field, forming fine fibers as the solution jets onto a collector. Electrospinning enables the creation of MOF-polymer and MOF-COF composite fibers with high surface area, uniform morphology, and enhanced mechanical properties. These fibers are beneficial for applications in energy devices, offering a scaffold that combines structural support with the functional properties of MOFs or COFs.[94–97]

4. Working mechanism of PENG and TENG

PENG works by applying mechanical stress or pressure to a piezoelectric material generates a change in the material's internal polarisation. This polarisation shift causes an electric potential differential across the material. The applied mechanical force separates the positive and negative charge centres inside the piezoelectric crystal structure. This charge separation generates an electric field, which may be converted into electrical energy. As the mechanical tension is relieved, the material recovers to its former condition, allowing the charges to flow back and generate an alternating current. This period process leads to the generation of electrical output using PENG device. The schematic illustration of the working mechanism of PENG is shown in Fig. 2(a).

TENG works based on contact electrification and electrostatic induction. There are four working modes in TENG, such as vertical contact-separation (VCS), lateral sliding (LS), single

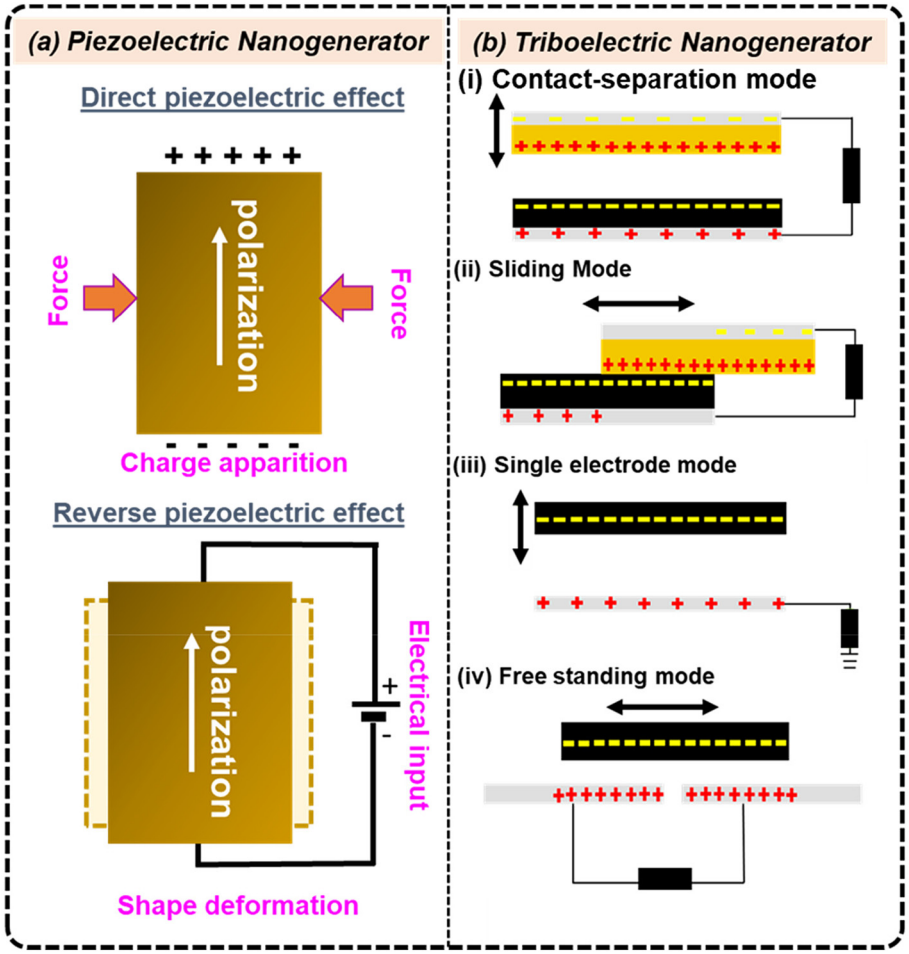

Fig. 2 (a) Working mechanism of piezoelectric nanogenerator, (b) various working modes of triboelectric nanogenerator (i) contact-separation mode, (ii) sliding mode, (iii) single-electrode mode, (iv) free standing mode.

electrode (SE) and free-standing triboelectric layer mode. VCS mode where two distinct materials come into contact and then separate. Due to triboelectric effect charge transfer across their surfaces when they come into contact. As they parted ways, an electric potential difference is formed, which causes electrons to flow between the electrodes to balance the potential, resulting in alternative current. In LS mode, two materials moving against each other laterally. The sliding action creates charge transfer in the contact area. As the contact area changes during sliding, a potential difference develops, causing electrons to flow between the electrodes and generate current. SE configuration just one electrode is linked to the electrical measuring system or load, leaving the other floating or grounded. When the triboelectric layer moves relative to the single electrode, it generates an electric field that causes a potential difference, allowing electrons to flow between the electrode and the ground. Free standing mode employs a dynamic triboelectric layer that interacts with two fixed electrodes. As the freestanding layer travels between the electrodes, it causes charge transfer and generates a potential difference, which drives current flow. Various working modes of TENG is illustrated in Fig. 2(b).

The influence of MOFs and COFs on triboelectric nanogenerators and piezoelectric nanogenerators largely stems from their ability to modulate surface properties through donor–acceptor interactions and tailored electronic structures.[98–100] MOFs and COFs are porous crystalline materials with customizable architectures, allowing for precise incorporation of donor or acceptor functional groups. These groups create localized regions of positive and negative charge, which significantly impact surface polarity, charge separation, and electron transfer—all essential factors for efficient energy harvesting in TENGs and PENGs. The existence of donor–acceptor pairs in MOFs/COFs improves the capacity of material to give or receive electrons upon contact with other surfaces, which is important in TENGs where contact electrification and electrostatic induction are essential. By improving the triboelectric effect and increasing charge density, this customized surface contact raises the output voltage and current. MOFs/COFs can be designed to enhance charge mobility and retention by adding

electron-donating or electron-withdrawing groups, which will result in a more effective charge transfer process. Similarly, the electronic structure of MOFs/COFs is crucial in PENGs, which use piezoelectric phenomena to transform mechanical stress into electrical energy. Donor–acceptor interactions affect the polarization of framework materials, enabling regulated charge separation during deformation. Furthermore, wide surface area and adjustable pore structure of framework materials promote mechanical flexibility and increased surface interaction, which enhances their effectiveness in energy harvesting applications. Overall, the donor–acceptor interactions in MOFs/COFs provide precise control over surface charge characteristics, which directly improves the performance of both TENG and PENG devices. Because of this, MOFs and COFs are extremely valuable and adaptable when creating high-output, flexible, and efficient energy harvesting systems. Tuning the work function of materials for TENG and PENG nanogenerators is key to enhancing their efficiency.[101–103] Adjusting the work function involves surface modifications and doping to tailor electron affinity and enhance charge transfer efficiency. Incorporating electron-donating or -withdrawing groups, such as fluorine or nitrogen, can shift the work function by altering the electron density at the surface. Additionally, controlling the crystallinity and surface roughness affects charge distribution and enhances triboelectric performance. Hybridizing materials (*e.g.*, metal–organic frameworks with polymers) or forming composites can further adjust the work function, creating optimal charge exchange conditions. These methods enable fine-tuning for targeted energy applications.

5. Energy harvesting using framework materials

5.1. Energy harvesting using MOFs

In the previous section, we discussed about how MOFs are excellent as active material for TENGs, which can generate energy from the environment. This is due to their high surface area, porosity, and high chemical and thermal stability. Wang *et al.* proposed the strong electron-withdrawing group (EWG) F modified UiO-66-4 F as a potential material for developing and using high-performance MOF-based TENG devices.[104] The parent MOF is UiO-66(Zr). UiO-66-NH_2 and UiO-66-4F is the family member of Zr based MOF. By modifying the functional group of these materials, we can alter its properties and output values. Earlier this group also reported MOF based TENG using UiO-66-NH_2 with PDMS composite material and reported the output voltage and current had improved 4 and 60 times respectively as compared to the PDMS based TENG. Wang *et al.* also examined that the effect of EWG enhanced the surface potential and surface roughness, which is main parameter for TENG.[105] Here this team introduced another modified UiO-66 MOF that is UiO-66-4 F which adopts an easy synthesis procedure with water at room temperature. The structure is made up of $Zr_6O_4(OH)_4$ and 12 tetrafluoro terephthalic acid ligands, each containing four F atoms. The high amount of fluorine gives it a strong ability to attract and hold onto electrons. This deliberate design choice imparts a robust electron-withdrawing ability to UiO-66-4F, thereby significantly enhancing its charge-inducing and charge-trapping capabilities compared to the unmodified UiO-66. Mixing MOF particles into PDMS, is a simple way to change the surface roughness which can hold an electrical charge and can act as an insulator. It also alters the surface potential and dielectric constants. KPFM is used to verify the surface alterations made to the customized composite. KPFM studies showed that adding just 9% of UiO-66-4F to PDMS greatly reduced its surface potential from −1.4 V to −6.0 V and made it rougher. As a result, the TENG made with UiO-66-4F and PDMS could produce a maximum voltage of 937.4 V, a current of 30.6 μA, and a power density of 38.7 W m^{-2} and greatly improved the range and effectiveness of TENGs is shown in Fig. 3 (a-b). These results highlight how well the newly developed MOF-based composite works to improve TENGs' capacity for energy collecting.

Shaukat *et al.* introduced a novel TENG device using MOF-5, paired with PTFE as the counteracting triboelectric layer is shown in Fig. 3(c).[59] MOF-5 stands as a well-established member within the MOF family. Its structure is characterized by a three-dimensional configuration, where $[Zn_4O]^{6+}$ inorganic clusters connect with an octahedral arrangement of $[O_2C\text{-}C_6H_4\text{-}CO_2]_2$ (H_2BDC) groups in the PCU topology. This connectivity results in the creation of a highly porous space group structure ($Fm\bar{3}m$). The distinctive architecture of MOF-5 contributes to its remarkable surface area and substantial pore volume. MOF-5 was synthesized employing a hydrothermal technique utilizing Zinc nitrate hexahydrate and terephthalic acid as initial precursors, while DMF served as the solvent. Subsequently, the resultant solution was subjected to an oven at a temperature of 100 °C for 24 hours. The ensuing powder was cleansed using DMF and acquired through centrifugation. Lastly, the resultant white precipitate was desiccated in ambient air for a period of 24 hours. This study marks the first instance of employing MOF-5 in the creation of both TENG and PENG aimed at energy harvesting. The device showcased impressive output, generating an open-circuit voltage of 484 V, a short-circuit current of 40 μA, and a peak instantaneous power of 3174 μW, even in challenging environmental conditions. The TENG was effectively used to charge various commercial capacitors, power LEDs, and operate low-energy electronics like calculators and stopwatches. Furthermore, the research delved into using MOF-5 for developing PENG. These findings suggest that MOF-5 is not only suitable for crafting highly durable TENGs for extreme environments but also holds potential in the realm of PENG.

In material science, precise manipulation of crystalline structures is a crucial strategy for enhancing the fundamental performance of solid materials. This is particularly evident in MOFs, where structural control can be achieved through reversible cation-exchange, influencing their single-crystal-to-single-crystal (SC–SC). Huang *et al.* reported a study on a TENG device, focusing on the reversible structural change between a zinc-

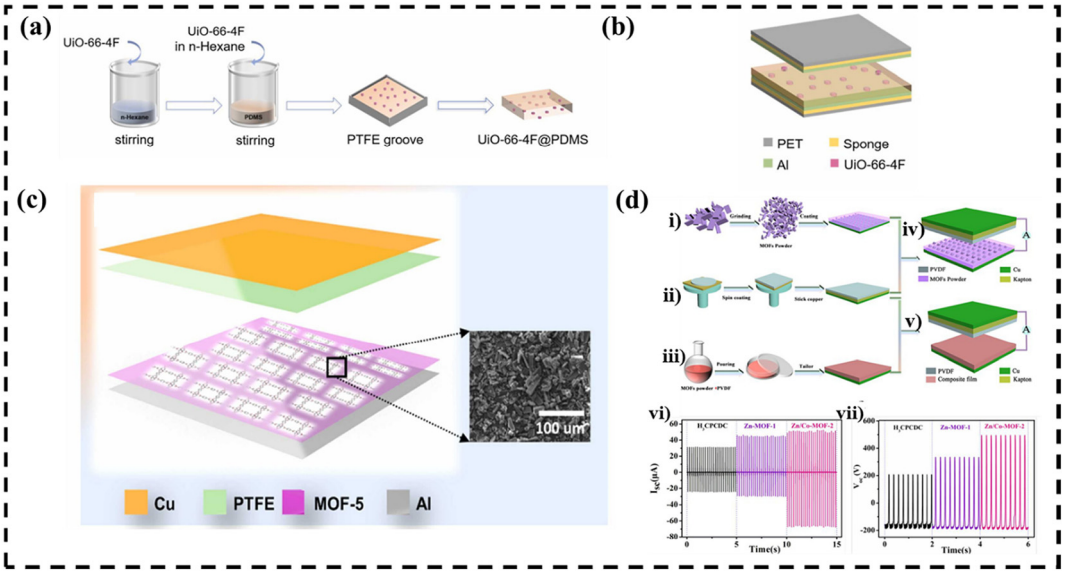

Fig. 3 (a) Preparation procedure of UiO-66-4F@PDMS composite films. (b) The structure diagram of the UiO-66-4F@PDMS TENG device.[104] (c) The schematic diagram of the proposed based MOF-5-based TENG device. Reprinted from ref. 59 Copyright © 2022, Elsevier. (d) Schematic representation of the preparation of (i, ii, and iv) MOF-based TENG and (ii, iii and v) MOF@PVDF film-based TENG. The output performances (I_{sc} and V_{oc}) of power MOF-based TENGs: (vi and vii) I_{sc} and V_{oc} of H3CPCDC-, Zn-MOF-, and Zn/Co-MOF-TENG, respectively. Reprinted from ref. 106. Copyright © 2022 American Chemical Society.

based MOF (1) and its structurally similar bimetallic version, a zinc/cobalt MOF (2).[106] This transformation, visible to the naked eye, is driven by a single crystal to single crystal (SC–SC) process, marking a significant stride in the field. Both MOFs, in their powdered forms and as part of hybrid composites, were utilized as positive electrode materials in the assembly of TENGs. The integration of Co ions into the Zn-MOF structure not only facilitated easier electron transfer but also significantly enhanced the output performance of the resulting Zn/Co-MOF-TENG is shown in Fig. 3(d). This was evidenced by the substantial increase in short-circuit current (I_{sc}), charge density (σ), and open-circuit voltage of the Zn/Co-MOF-TENG, showing improvements of approximately 50.62%, 77.24%, and 21.94%, respectively, compared to the Zn-MOF-TENG. They also further investigated by using MOF@PVDF (polyvinylidene fluoride) composite film-based TENGs. These tests revealed that the Zn/Co-MOF@PVDF-TENG demonstrated the highest output performance among all the assembled TENGs. This superior output was not only consistent but also stable, as showcased in its application to power an ultraviolet lamp plate for the photochemical cycloaddition of organometallic macrocycles. The successful application of this technique in improving the output performance of MOF-based TENGs opens up new avenues in the design and utilization of MOFs as advanced materials in energy harvesting and other technological applications.

Recent studies have introduced the biodegradable metal–organic framework (MOF) MIL-88A as a groundbreaking material for TENG, named MIL-TENG. This eco-friendly MOF is synthesized using iron chloride and fumaric acid in water, at 65 °C for 4 h by following a hydrothermal synthesis procedure, highlighting its environmentally friendly production process. Khandelwal *et al.* reported MIL 88A based TENG device in which the triboelectric performance of MIL-88A was assessed by pairing it with various materials, revealing a distinct output trend: TENG with ethyl cellulose (EC) < TENG with Kapton < TENG with fluorinated ethylene propylene (FEP) is shown in Fig. 4(a).[107] This TENG harvest energy *via* coupling of contact electrification and electrostatic induction. Notably, the combination of MIL-88A and FEP exhibited impressive electrical outputs, generating an output voltage of 80 V and an output current of 2.2 mA. These results underscore the positive triboelectric behaviour of MIL-88A, particularly in relation to FEP and Kapton. Surface potential measurements further corroborate the advantageous triboelectric properties of MIL-88A. The MIL-TENG, especially with FEP as the counter layer, demonstrates its capability for efficient energy harvesting through contact electrification and electrostatic induction. The positive electrostatic surface potential of MIL-88A indicates its suitability as a non-toxic, multifunctional material for TENG applications. In practical scenarios, the MIL-TENG has been successfully employed for biomechanical energy harvesting and for powering a range of low-energy electronic devices through a capacitor Fig. 4(b). This development not only showcases the potential of MIL-88A in energy harvesting applications but also contributes to the growing field of sustainable and environmentally friendly energy technologies.

Recent advancements in green energy technologies have been bolstered by the introduction of cyclodextrin-based metal–organic frameworks (CD-MOFs) in the realm of TENGs. Hajra *et al.* reported the development of an economical method to synthesize biocompatible cyclodextrin MOFs at room temperature.[58] The research highlights the development

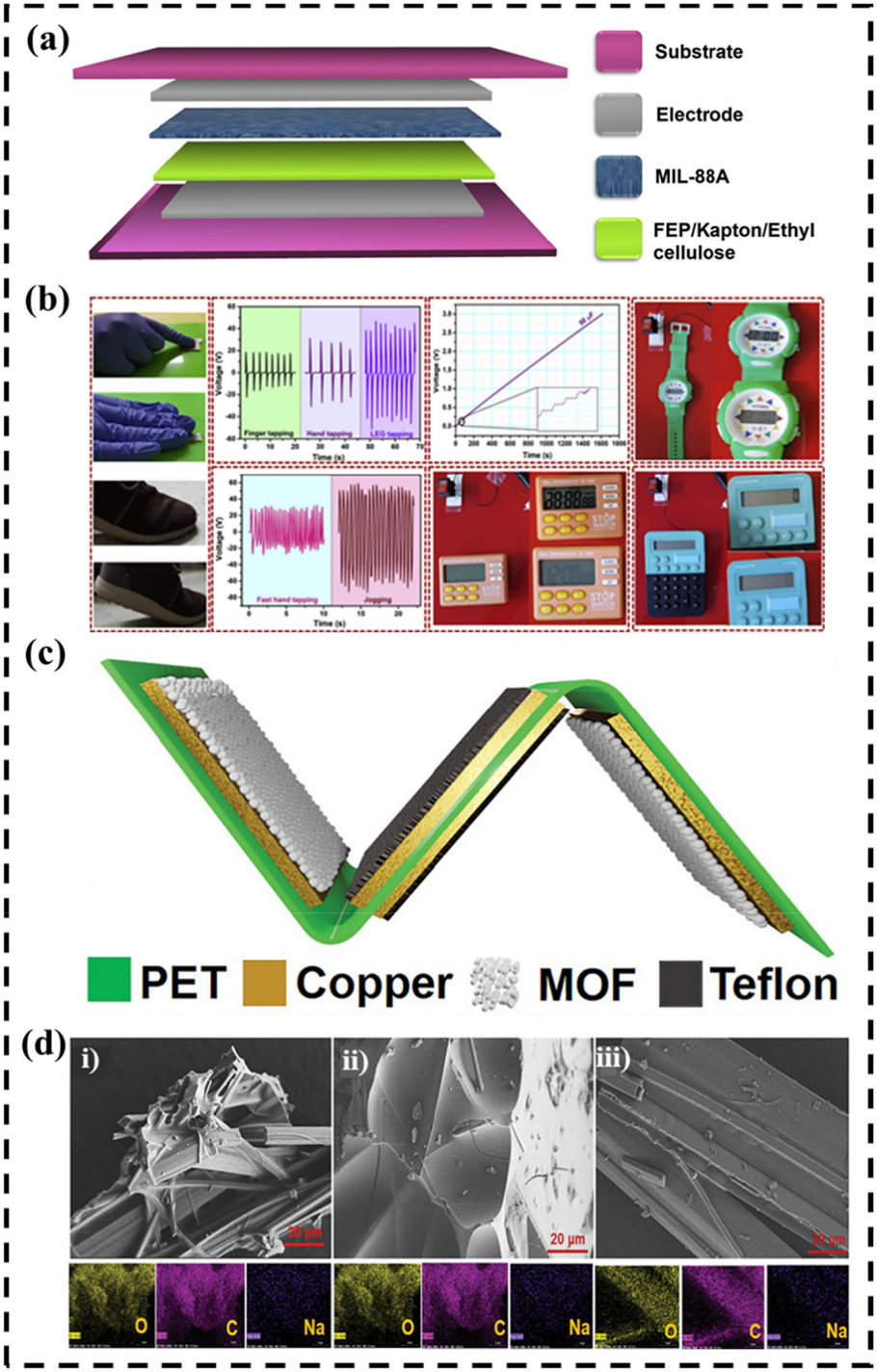

Fig. 4 (a) The 3D exploded view of MIL-TENG. (b) Biomechanical energy harvesting and driving low-power electronics. Reprinted from ref. 107, Creative Commons CC-BY-NC-ND © 2022, The Author (s). (c) The illustration of the multiunit-based vertical contact and separate TENG device. (d) (i–iii) SEM and color mapping of the alpha, beta, and gamma CD-MOF. Reprinted from ref. 58.Copyright © 2021 Wiley-VCH GmbH.

of CD-MOFs utilizing cyclodextrin as an organic ligand and sodium as a metal ion. These CD-MOFs are synthesized through an ultrasonic method and are notable for their non-toxicity, biocompatibility, and edibility, marking them as environmentally friendly multifunctional materials. The synthesis of CD-MOF (alpha, beta, and gamma) through ultrasonic methods was conducted using a straightforward and scalable route. Cyclodextrin particles and sodium bicarbonate were combined in water in a glass beaker, subjected to ultrasonication for 10 minutes. Trimesic acid was then added to the homogeneous solution and left for 24 hours, followed by an additional 10 minute ultrasonication period. The collected

material underwent multiple washes with DMF and was subsequently dried in a convection oven. The study focuses on three types of CD-MOFs: alpha, beta, and gamma, whose surface potential has been evaluated using KPFM. This assessment revealed their positive surface potential, influencing their triboelectric output. Among these, the alpha CD-MOF, in combination with Teflon is shown in Fig. 4(c) exhibited superior performance, producing an electrical output of 152 V, 1.2 μA, and 14.3 nC.

This device was successfully integrated into everyday objects like shoe heels and school bags, showcasing its potential in harvesting energy from common movements such as walking, running, and bending. By using scanning electron microscope (SEM) the morphological properties of alpha, beta and gamma CD-MOFs are studied is shown in Fig. 4(d). This research marks a significant milestone in the field of energy harvesting, being the first to explore the use of biocompatible CD-MOFs (alpha, beta, gamma) for this purpose. The process involved pressing these CD-MOFs onto electrodes and analysing their surface potential and roughness profile. The KPFM investigations confirmed the placement of CD-MOFs within the triboelectric series and highlighted their compatibility with various triboelectric materials and positions them as a promising solution in the field of sustainable energy technologies.

Swain *et al.* has innovatively repurposed a spent petroleum catalyst, specifically Mo–Ni/Al_2O_3, to create a MOF for a TENG.[108] They successfully extracted MoO_3 from the spent catalyst and employed it as the metal ion, pairing it with Imidazole as the organic linker, to synthesize the Mo-MOF. The Mo-MOF was synthesised in a very simple and cost-effective way. A homogeneous mixture solution of MoO_3 and imidazole were prepared in deionized water and stirred. The resulting mixture was refluxed for 15 hours at 120 °C to yield the Mo-MOF. Subsequently, the product was washed three times with deionized water and dried. The MOF synthesised using this procedure gives a wedge shape rod like structure. In this MOF based TENG Mo-MOF is used as positive layer and Kapton as negative layer. This triboelectric potential was verified using KPFM technique which has average potential of 240 mV. The surface potential of Mo-MOF facilitates effective charge separation, resulting in increased output voltages. This TENG operated in the vertical contact and separation mode. When Mo-MOF combined with Kapton, this Mo-MOF-based TENG can produce an output of 148 V, a current of 470 nA, and a charge accumulation of 17 nC. This output is effectively harnessed to charge capacitors and power electronic devices. Notably, this TENG also finds application in monitoring repetitive motions such as boxing punches, showcasing its potential in the realms of intelligent sports and healthcare monitoring.

5.2. Energy harvesting using ZIFs

ZIFs are typically synthesized by reacting suitable hydrated metal salts, predominantly zinc and other metals favouring tetrahedral coordination, with an imidazole or its functionalized variants in an amide solvent like DMF or DEF. This process occurs at temperatures between 85 to 150 °C. ZIF-8 features a structure where Zn^{2+} ions are tetrahedrally connected to 2-methyl imidazole, forming a compound with the general formula Zn(2mIm). The architecture of ZIF-8 is based on a sodalite topology (**SOD** or sod), named after the mineral sodalite. In ZIF-8's structure, the **tro** cages measure 11.6 Å in diameter and are composed of 4- to 6-membered rings merged along their edges. ZIFs have been identified as promising materials for energy harvesting applications. These nanoporous crystalline materials possess a low dielectric permittivity, making them favourable for piezoelectric energy harvesting. The piezoelectric properties of ZIFs have been analysed, and it has been found that the variation of different building blocks of the structure, such as metal node and linker substituents, affect the piezoelectric constants. The piezoelectric tensor for ZIFs can be computed using *ab initio* theoretical methods, and the resultant piezoelectric coefficient has been found to vary significantly among different ZIF structures.[109]

The field of energy harvesting has witnessed a significant breakthrough with the introduction of a novel TENG by Khandelwal *et al.*, utilizing MOFs.[110] This innovative MOF-TENG capitalizes on the principles of contact electrification and electrostatic induction, presenting a straightforward and economical approach to convert waste energy into usable electrical power. Central to this development is the employment of the ZIF-8 in conjunction with Kapton to create the active layers of the MOF-TENG is shown in Fig. 5(a). Comprehensive investigations, encompassing surface potential assessments, structural and electrical analyses, have been conducted to elucidate the properties of ZIF-8. These studies, particularly employing KPFM, have affirmed the positive triboelectric nature of ZIF-8, positioning it as a strong contender for TENG applications. The MOF-TENG, fabricated in a conventional vertical contact-separation configuration, utilizes ZIF-8 and Kapton as the respective positive and negative triboelectric layers. This design has yielded a remarkable sustainable output, generating up to 164 V and 7 μA. A notable innovation includes the development of a self-powered UV counterfeit detection system and a highly selective, reusable tetracycline sensor. The sensor's efficacy is enhanced by its ease of resetting through simple washing procedures. Moreover, the MOF-TENG has been adeptly integrated into a system for powering temperature and humidity sensors using a capacitor. Its versatility extends to wireless charging capabilities for lithium-ion batteries. These charged batteries have been effectively utilized to power a portable UV light-emitting diode (UV-LED) system, designed for authenticating currency notes and aiding in forensic investigations is shown in Fig. 5(b). Additionally, the unique properties of the MOF have been harnessed to create a tetracycline sensor with exceptional selectivity, underlining the specific binding capabilities of the MOF. Overall, this pioneering work by Khandelwal *et al.* not only highlights the potential of advanced materials in the fabrication of TENGs but also significantly broadens the scope of their applications.

Another ZIF-8 based TENG device was fabricated by Hajra *et al.* which has been utilized in self-powered sensing of balance through integration into a robotics system, in powering a wristwatch, and in biomechanical energy harvesting.[88] Zinc nitrate hexahydrate ($Zn(NO_3)_2{\cdot}6H_2O$) and 2-methyl-

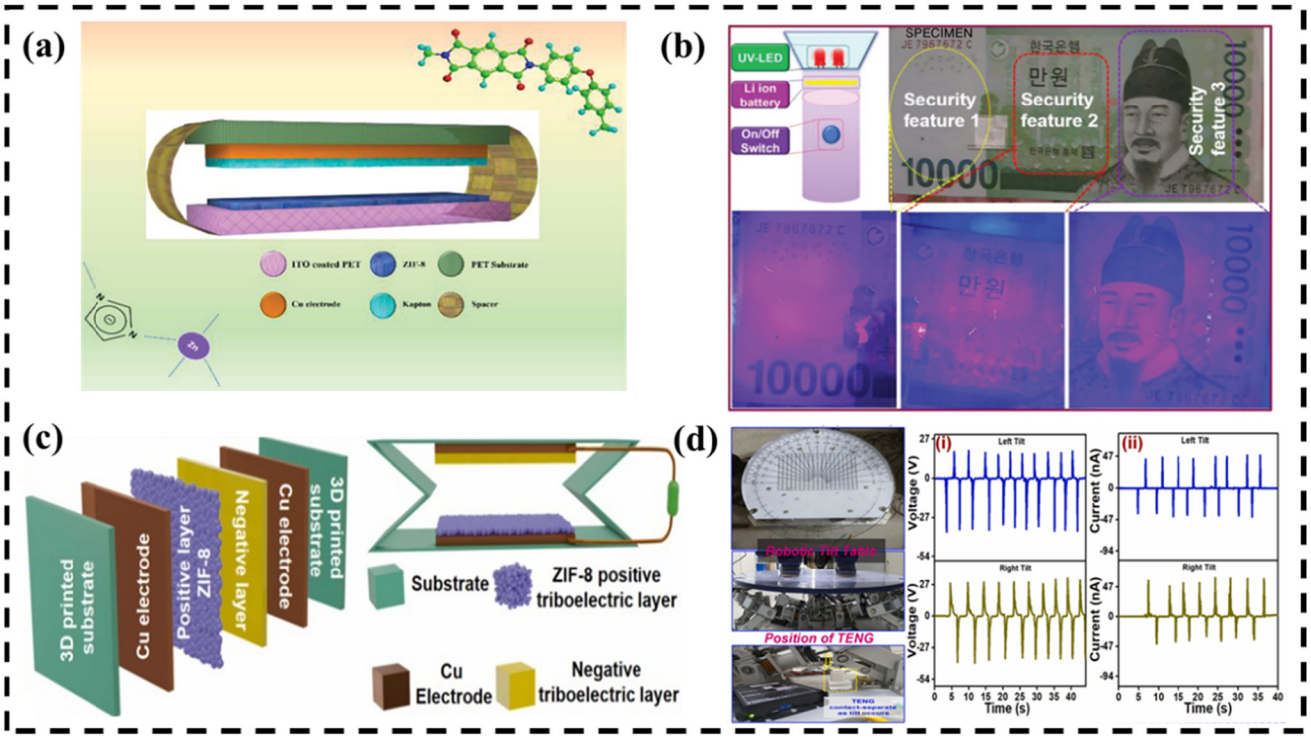

Fig. 5 (a) 3D schematic illustration of the designed MOF-TENG. (b) The designed self-powered UV counterfeit system is showing the three different areas for the security feature under UV light. Reprinted from ref. 110. Copyright © 2019, WILEY-VCH. (c) Illustration of the fabricated vertical contact separate mode TENG. (d) Digital images of the robotic tilt table, the person standing upon a robotic tilt table, and the position of the TENG to monitor the response during left and right tilt; (i and ii) voltage and current response of the single-unit ZIF-8 HG-kapton-based vertical contact separation mode TENG connected below the robotic tilt table. Reprinted from ref. 88 Copyright © 2022 Elsevier.

imidazole were solubilized in deionized water (DI H_2O) and agitated for a duration of 6 hours until a turbid white precipitate was formed. The precipitate was subsequently gathered and subjected to multiple washes with methanol to procure pure ZIF-8 crystals with a diameter measuring 205 nm. Conversely, ZnO was utilized as the metal precursor for the synthesis of ZIF-8 HG. A stoichiometric ratio of 2-methylimidazole and ZnO was introduced into an agate mortar and pestle, where they were subjected to grinding for a duration of 90 minutes. Samples were collected periodically, rinsed with hot water, and separated by centrifugation. Ultimately, the samples were subjected to drying at a temperature of 120 °C for a duration of 3 hours to obtain pure ZIF-8 crystals with a diameter measuring 230 nm. The successful synthesis of both the ZIF 8 SA and ZIF 8 HG was confirmed by various characterisation techniques. The microstructure analysis of both ZIF-8 HG and SA samples indicates the existence of nearly uniform rhombic dodecahedral-shaped crystals. It was noted that the surface potential and surface roughness of the ZIF-8 SA and ZIF-8 HG samples were measured as follows: 507 mV and 44.4 nm for ZIF-8 SA, and 717 mV and 94 nm for ZIF-8 HG, respectively by using KPFM technique. The voltage output of the single-electrode mode device was demonstrated by altering the composition of the free-moving layer. The free-moving layer is comprised of the combination of Kapton, PET and aluminium foil is shown in Fig. 5(c). The voltage, current and charge output of ZIF 8 HG is 150 V, 3.6 μA, 17 nC while 50 v, 1.4 μA and 30 nC for ZIF 8 SA. The ZIF-8 HG-Kapton TENG achieves the highest power output, reaching 62.42 μW at a 100 MΩ load resistance, whereas the ZIF-8 SA-Kapton TENG demonstrates a power output of 5.9 μW. The multi-unit, the triple unit TENG was connected parallelly and giving the output voltage of 150 V and the current of 4.95 μA. The direct use of ZIF-8 powders as a triboelectric layer allowed for the comparison of the dual operating mode of TENG and various electrical outputs. The single unit ZIF-8 HG-Kapton based vertical contact mode TENG is utilised for the purpose of self-powered robotic sensing and to detect the left and right tilting motion of robotic system while the single electrode mode TENG were employed to harvest energy from biomechanical activity bag swinging is shown in Fig. 5(d). In contrast, the triple-unit ZIF-8 HG-Kapton vertical contact mode TENG was employed to illuminate a wristwatch as a sustainable power source. So overall the additive manufacturing plastic wastes were efficiently repurposed in the design of multi-unit TENG devices, potentially offering socio-economic benefits.

Methanol, widely used in various sectors including industry and medicine, poses significant health risks upon inhalation, including severe tissue damage or fatal outcomes. Detecting methanol concentration swiftly and accurately at room temperature is therefore of paramount importance. Gas sensors play a crucial role in monitoring environmental safety, specifi-

cally in detecting toxic gas concentrations.[111,112] Traditional gas sensors often depend on rechargeable batteries and specialized equipment, which can restrict their lifespan and versatility. To address these limitations, Ma *et al.* integrated a TENGs with gas sensors offers a pathway to developing self-powered gas detection systems.[113] Their group have developed a TENG based on spiky structured ZIF-8@ZnO, as shown in Fig. 6(a). This novel TENG not only efficiently harvests energy but also functions as an effective self-powered sensor for methanol. First, the synthesis of ZnO was conducted using $Zn(NO_3)_2{\cdot}6H_2O$ and NaOH as precursors. Both precursors were dissolved in DI water. The resulting solution was then agitated and transferred into a stainless-steel autoclave, where it was subjected to a temperature of 140 °C for a duration of 12 hours. Following this, the resultant white ZnO was collected and subjected to multiple washes with deionized water, after which it was dried at a temperature of 60 °C for a duration of 12 hours. Subsequently, for the synthesis of ZIF-8@ZnO, the previously synthesized ZnO was dispersed in dimethylformamide (DMF) and mixed with deionized water containing 2-methylimidazole. The resulting mixture was agitated for a period of 3 hours, during which it underwent a noticeable change in colour to milky white. The final product was then collected and subjected to multiple washes with deionized water and DMF. Following this, the ZIF-8@ZnO white powder was dried at a temperature of 105 °C in a vacuum oven for a duration of 12 hours and underwent a morphology test, as shown in Fig. 6(b). This TENG works on contact separation mode (Fig. 6c).

In this study, the ZIF-8@ZnO is employed as the positive layer, while PVDF serves as the negative layer. This strategic implementation leads to a notable enhancement in the overall output performances of TENGs based on ZIF-8@ZnO/PVDF. The resultant measurements indicate that the open voltage, short current, and transfer charge of ZIF-8@ZnO-based TENGs are approximately 58 V, 10 μA, and 25 nC, respectively, as shown in Fig. 6(d). The sensor exhibits high sensitivity and selectivity towards methanol gas at room temperature, a characteristic attributed to the porous structure of ZIF-8 and the heterostructure of ZIF-8@ZnO, as shown in Fig. 6(e). The response rate of the ZIF-8@ZnO-based TENG to 100 ppm methanol is impressive at 30.35%, with rapid response (~5.9 s) and recovery times (~2.2 s). The enhanced sensitivity and selectivity of the ZIF-8@ZnO-based TENG compared to bare ZnO-based TENGs can be credited to the porous nature of the ZIF-8 shell. This research not only underscores the potential of MOF-modified metal oxide semiconductors in self-powered gas sensing but also offers a promising strategy to improve the output performance and sensing capabilities of TENGs based on metal oxide semiconductors.

Hajra *et al.* reported the development of a TENG device based on ZIF-67, incorporating various negative triboelectric layers like Teflon, PDMS, and paper.[114] They introduced a novel S-shaped TENG device, known as S-TENG, which was designed using a simple vertical contact mode and fabricated through an additive manufacturing technique, as shown in Fig. 7(a). ZIF-67 was synthesized in a very easy and cost-effective way at room temperature. Co^{2+} and 2-methyl imidazole were mixed in proper ratio to form [Co(2mIM) IM = imidazolate]. A definite quantity of $Co(NO_3)_2{\cdot}6H_2O$ and 2-MIM were dissolved individually in methanol. Subsequently, the $Co(NO_3)_2{\cdot}6H_2O$ solution was gradually added to the 2-MIM solution while vigorously agitating. The resulting mixture was stirred at ambient temperature for a duration of 6 hours. Upon combination of the two solutions, a purple precipitate materialized. The particles were subsequently separated through the process of centrifugation. These particles underwent two rounds of methanol washing before being subsequently dried in an oven set at 60 degrees to get cubic shape structure, as shown in Fig. 7(b). In this device, ZIF-67 served as the positive triboelectric layer, while teflon/PDMS functioned as the negative triboelectric layer, as shown in Fig. 7(c). At a load resistance of 50 MΩ the S-TENG produced a voltage of 118 V, a current of 1.7 μA, and a power density of 15 μW cm^2. The multiunit S-TENG devices demonstrated a clear pattern in terms of their current and charge that can be used in self-powered gait monitoring (Fig. 7d). Specifically, the ZIF-67/teflon device had a current of 1.7 mA and a charge of 35 nC. In comparison, the ZIF-67/PDMS device had a current of 0.3 mA and a charge of 24 nC. Lastly, the ZIF-67/paper device had a current of 0.17 mA and a charge of 13 nC, as shown in Fig. 7(e). The ZIF 67/teflon based S-TENG device was effectively used to charge a commercial capacitor, which in turn powered a wristwatch. It was also integrated with a robotic gripper to aid in object identification (Fig. 7f).

Barsiwal and his team developed a cost-effective, straightforward, single-step approach to fabricate a TENG device, achieving remarkably efficient results.[83] In their design, they utilized ZIF-67 as positive triboelectric layer and PET and PMMA (polymethyl methacrylate) as the negative triboelectric layers. The TENG was subjected to a comparative evaluation against manual tapping. The testing process involved maintaining a constant triboelectric layer of ZIF-67 while introducing variations in the materials used, namely kapton, teflon, silicone, PET, and PMMA. The TENG device, particularly the PMMA/ZIF-67 combination, demonstrated outstanding output performance, with recorded values of 300 V in open-circuit voltage, 47.5 μA in short-circuit current, and a power density of 593 mW m^{-2}. The generated output from the TENG proved sufficient for activating various electronic devices, including a calculator, a digital watch, a digital thermometer, a series of 250 LEDs, as well as an electroluminescent (EL) device.

Khandelwal *et al.* have developed a series of ZIF for TENG applications. The research team successfully synthesized a series of mixed linker MOFs within the ZIF category, including ZIF-62, ZIF-7, ZIF-9, ZIF-11, and ZIF-12 and published several articles.[115] ZIF-62, a mixed linker ZIF subfamily member, as an active component in TENG devices. ZIF-62, comprising imidazole (Im) and benzimidazole (bIm) linkers, adopts a Cag topology. This MOF features two distinct zinc atoms, each coordinated to one disordered linker and three Im linkers. ZIF-7 and ZIF-9 exhibit a sodalite (**SOD**) topology; ZIF-7 is structured

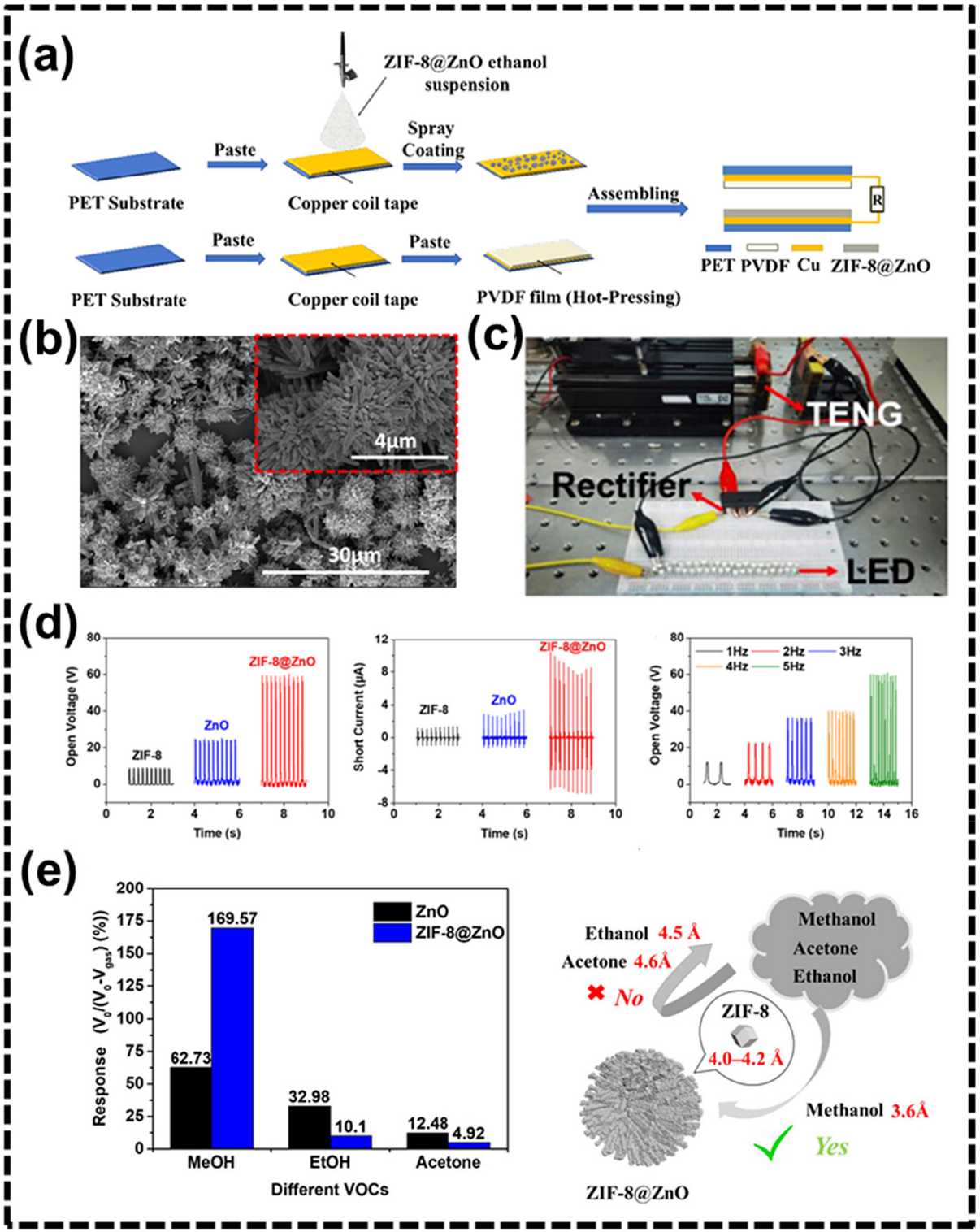

Fig. 6 (a) Scheme of illustration of the fabrication process of the ZIF-8@ZnO/PVDF TENG (b) SEM images of ZnO with different magnifications; (c) the optical diagram of the circuit of ZIF-8@ZnO/PVDF TENGs for illumination of commercial LEDs; (d) comparison of open voltages and short current (μA) at 5 Hz of ZIF-8, ZnO and ZIF-8@ZnO-based TENGs and comparison of open voltages of ZIF-8@ZnO TENGs with different frequencies; (e) comparison of responses of ZnO and ZIF-8@ZnO to methanol, ethanol, and acetone and schematic illustration for the mechanism of the selective methanol sensing of ZIF-8@ZnO. Reprinted from ref. 113 Copyright © 2023, American Chemical Society.

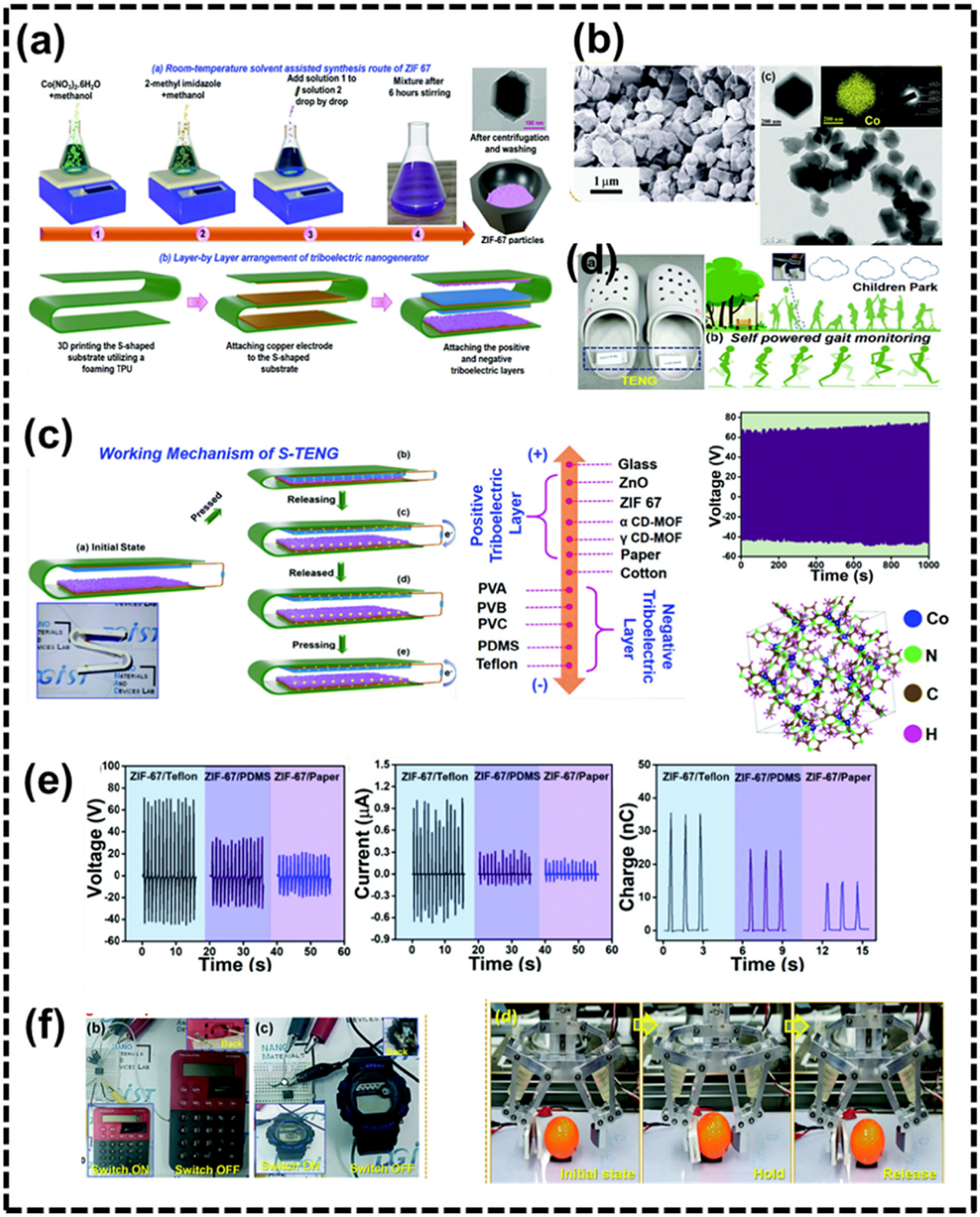

Fig. 7 (a) Synthesis of ZIF-67 particles and layer-by-layer arrangement for fabrication of the S-TENG device (b) surface micrographs and HRTEM image and (inset) image of a single ZIF-67 particle, mapping analysis of Co and SAED patterns of the ZIF-67 sample; (c) digital image of the S-TENG attached to shoes and the table showing standard and mean deviation of different types of gaits of volunteers; (d) digital image of the switch ON–OFF of a calculator, digital image of the switch ON–OFF of a wrist-watch and digital images of the initial state, hold, and release condition of a golf ball using a robotic gripper; (e) working mechanism of the S-TENG device, triboelectric series and the position of positive and negative polarity of materials, stability test of the S-TENG device for 1000 seconds and chemical structure of ZIF-67 and (f) voltage, current, and charge comparison of the S-TENG device based on ZIF-67 as a positive triboelectric layer and alternating the opposite triboelectric layers Teflon, PDMS, and paper. Reprinted from ref. 114, Copyright © 2021, Royal Society of Chemistry.

with divalent zinc cations (Zn^{2+}) interconnected by bIm anions, whereas ZIF-9 employs bIm as the linker with cobalt (Co^{2+}) as the metal ion forming hexagonal symmetry. The three-dimensional structures of ZIF-11 and ZIF-12 are defined by a **RHO** topology, in which zinc ions in ZIF-11 and cobalt ions in ZIF-12 are each coordinated to four nitrogen atoms of the bIm linker and adopts cubic structure. ZIF-11 features larger cages in comparison to ZIF-7. Utilizing KPFM and surface potential assessments, the team identified a positive potential on the ZIF family members. The surface voltmeter confirmed the positive triboelectric nature of ZIF-62, exhibiting a surface potential of 0.6 V. The open-circuit voltage of the ZIF-62 TENG is reaching a maximum output of 80 V under open circuit conditions. Additionally, device performance was boosted by ion deposition using a Zerostat 3 anti-static gun, resulting in an output voltage of 175 V and a current of 10 μA. The device maintained this output for over 20 hours before beginning to decline after 21 hours, with an endurance test lasting up to 29 hours revealing reduced output but continued functionality. The device demonstrated a maximum peak power of 6.05 μW and a power density of 9.68 mW m^{-2} across a 500 MΩ load. The device is used to charging capacitors up to 3 V showing that a 1 μF capacitor took the longest time due to its high capacitance. Moreover, the fabricated device was utilized for fitness tracking during various gym exercises such as hand curls, squats, and shoulder presses. Finally, a range of low-power electronics including green LEDs, thermometers, wristwatches, calculators, and ultraviolet LEDs were successfully powered by the ZIF-62-TENG device. Additionally impact of moisture on device output performance was also tested, revealing consistent output even at 60% relative humidity (RH), with only a slight decrease observed at 80% RH. Finally, the device powered various low-rating electronics including wristwatches, calculators, hygro-thermometers, ultraviolet (UV), and infrared (IR) light-emitting diodes (LEDs). This study underscores the potential of ZIF family members to expand the triboelectric series and pave the way for the development of highly selective self-powered sensors and systems in the future. Nitha *et al.* developed a novel TENG by decorating ZIF-67 onto a fingerprint-mimicking Ecoflex.[116] The study focused on improving the performance of the TENG through the integration of the distinctive characteristics of ZIF-67 with the fingerprint-like structure of the Ecoflex film. The composite structure was developed to enhance charge generation and retention, which could result in more effective energy harvesting from mechanical motion. The fabricated TENG generated an output of 401 V and 12.8 μA respectively. The device was incorporated into a smart glove system linked to IoT cloud services, tailored for the care of paralyzed patients. Sarfudeen *et al.* synthesized a zeolitic tetrazolate framework (ZTF-8) through the ball milling process.[117] This material, exhibiting structural similarities to ZIF-8, was employed in the development of a TENG. The ZTF-8-based TENG exhibited remarkable performance, achieving a power density of 720 mW m^{-2}, capable of powering devices such as tally counters, clinical thermometers, and digital clocks, in addition to illuminating 125 LEDs. The ZTF-TENG served as a self-powered selective dopamine sensor, demonstrating impressive sensitivity, extensive linearity (5–120 μM), and a remarkable detection limit (0.42 μM). This novel method integrates the distinctive characteristics of ZTF-8 with TENG technology, leading to a multifunctional device capable of converting mechanical energy into electricity while also functioning as a sensitive neurochemical sensor. Bariswal *et al.* designed a TENG using ZIF-67 as the positive triboelectric layer and polymethyl methacrylate (PMMA) as the negative layer.[118] The device is operated in contact separate process and achieved an open-circuit voltage of 300 V, a short-circuit current of 47.5 μA, and a maximum power density of 593 mW m^{-2}. The team showcased the practical applications of their TENG by successfully illuminating 250 LEDs. Additionally, the exploration of its potential for self-powered devices highlighted its versatility and efficiency in converting mechanical energy into electrical power. Memon *et al.* created a TENG utilizing ZIF-67 ink and PVDF ink as tribolayers through the electrohydrodynamic (E.H.D) method.[119] The device was operated in contact separation mode, yielding an output voltage of 119.6 V and a current of 7.7 μA, along with a power density of 171 mW m^{-2} at a load resistance of 60 MΩ. The duality of this TENG was evaluated for pressure sensing at low pressure, delivering a sensitivity of 3.392 V kPa^{-1}, a response time of 10 ms, and durability of up to 10 000 cycles for pressures reaching 3.1 kPa. This TENG demonstrates significant potential for integration as a power source in micro-based circuit device applications, while also serving a dual purpose as a pressure-sensing device within advanced miniature technology. Abbas and the team optimized the NH_2-Zn-MOF based nanogenerator using the first principle theory to enhance triboelectrification.[120] They incorporated amine functional groups into the organic linkers of the MOF to increase its electron-donating capability. The amine functionalization of the Zn-MOF resulted in alterations to the surface charge density and dielectric properties. The amine group functions as an electron donor in relation to the opposing layers, which exhibit electron-withdrawing characteristics. Through the application of reticular chemistry, these organic ligands can be modified *via* pre/post synthetic techniques to change the tribo-charges. The V-shaped NH2-Zn-MOF-based TENG reached a peak-to-peak voltage of 624 V and exhibited a current density of 1.28 mA m^{-2}. The developed TENG served as a potential energy harvester for low-power electronics and smart sports sensors. Similarly, Abbas *et al.* developed a MOF-based TENG to enhance triboelectrification and charge trapping effects, utilizing a newly synthesized Cd-MOF.[121] A composite film was utilized to fabricate the MOF-TENG, incorporating Cd-MOF and PDMS. The constructed device produced an impressive output of 193.4 V and 0.86 μA, achieving a peak power density of 0.124 W m^{-2}. The KPFM analysis indicates that the MOF/PDMS composite exhibits a significant surface charge and experiences minimal charge decay. Therefore, the achieved performance results from the charge trapping effect and enhanced surface charge. The MOF-TENG device was utilized to create an innovative tool known as an air mouse,

which operates by affixing the device to the fingers and navigating the mouse pointer through finger movements. It facilitated the harvesting of biomechanical energy and enabled exercise monitoring.

5.3. Energy harvesting using COFs

COF materials offer numerous advantages, such as 2D sheet structures and a network of parallel layers, which provide a robust skeletal framework ideal for high-performance energy harvesting devices.[6] Their potential as a triboelectric layer is notable, as COFs support charge transfer through skeleton-like pathways, surface roughness, and a relatively higher surface potential compared to other organic or inorganic materials. This makes them a significant contender for TENG fabrication.

In a recent work, Hajra *et al.* reported a novel COFs featuring a triazine skeleton and their energy harvesting capabilities were explored. [17] This research focuses on utilizing a nitrogen-rich organic moiety based on triazine for COF synthesis, followed by evaluating its surface potential and roughness using Kelvin probe force microscopy, which are critical factors in determining their position in the triboelectric series, as shown in Fig. 8(a). The COF was synthesised using a Schlenk tube equipped with a condenser and magnetic stirring bar. The tube is filled with 315 mg (2.485 mmol) of melamine and 500 mg (3.728 mmol) of terephthaldehyde, followed by the addition of 20 ml dry DMSO. After degassing with Nitrogen and stirring for 20 minutes at room temperature, the clear solution is heated at 180 °C for 72 hours in an inert atmosphere. The resulting solid is then cooled, washed with acetone through centrifugation, and dried at 70 °C under vacuum for 24 hours to obtain the desired product. Considering the COF layer as a potential candidate to serve as a triboelectric layer in expanding the conventional triboelectric series, the experimental average surface roughness was determined to be 112 nm, with a surface potential of 2.03 V. They fabricated the TENG device structure by using the as synthesized COF layer as a positive triboelectric component, with the innovation facilitated by 3D printing technology, aiming to optimize energy harvesting efficiency, as shown in Fig. 8(b). The results revealed an exceptionally high positive triboelectric potential of 2.03 V, indicating the material's promising capabilities. The electrical output performance of a single unit of the COF-based TENG demonstrated outputs of 70 V, 0.6 μA, and 38 nC (Fig. 8c). For enhanced performance, the study explored multiunit TENG configurations which significantly amplifies the current and voltage output from a single unit to four units connected in series and parallel. Multiunit TENG exhibited a significant boost in peak-to-peak current output, resulting in a 6.3 μA increase and yielded a voltage of 175 V. This work not only details the synthesis of nitrogen-rich COF material and the fabrication of the TENG but also opens avenues for the creation of low-cost self-powered hand-strengthening devices and serving as a beneficial tool for stroke patients dealing with finger extensor weakness or flexor dysfunction, as shown in Fig. 8(d).

Shi *et al.* developed a novel high-performance TENGs by using highly fluorinated Tp-TFAB COF designed from 1,3,5-tris (2,3,5,6-tetrafluoroaniline) benzene (TFAB) and triformylphloroglucinol (Tp) [122]. The Tp-TFAB COF was synthesized by using a solvothermal route. For comparison study, they also synthesized a non-fluorinated Tp-TAPB COF, made from 1,3,5-tris(4-aminophenyl)benzene (TAPB). The successful synthesis of both the COF was characterized by PXRD, ^{13}C NMR, N_2 adsorption–desorption isotherm and TGA. To explore the triboelectric properties of Tp-TAPB and Tp-TFAB COFs their respective powders attached uniformly to Ni tape as one triboelectric layer. Simultaneously, PVC films with nanopores were utilized as the opposing triboelectric layer in the construction of vertical contact-separation mode TENGs. The TENGs were evaluated under fixed conditions: a contact force of 40 N, a spacer distance of 4 mm, and a working frequency of 4 Hz. When connected to the positive side of the electrometer, both PVC-Tp TAPB and PVC-Tp TFAB TENGs exhibited a positive transferred charge output signal, indicating the positive triboelectric nature of pure Tp-TAPB and Tp-TFAB COFs. PVC- Tp-TFAB TENGs showed significantly higher triboelectric output than PVC-Tp TABP TENGs, with peak short-circuit current density (J_{sc}) increasing from 9.15 to 16.25 mA m^{-2}, transferred charge density (Q_{sc}) changing from 70.4 to 94.6 μC m^{-2}, and output voltage (V_{oc}) rising from 99.8 V to 137.8 V. This new Tp-TFAB COF exhibits superior triboelectric capabilities compared to the non-fluorinated Tp-TAPB COF as fluorine groups having strong electron-withdrawing ability it increases the electron donating ability of Tp-TFAB COF confirming electron transfer during triboelectrification. The PVC-PVA/Tp-TFAB TENG produces impressive triboelectric outputs, with a short-circuit current density of 26.34 mA m^{-2}, a charge transfer density of 148.5 μC m^{-2}, and a peak power density reaching 8.24 W m^{-2} which is almost sixfold greater than the PVC-PVA TENG. Under optimal conditions, the PVC-PVA/Tp-TFAB TENG can harvest 32.02 μJ of energy per cycle, achieving an average output power density of 320.2 mW m^{-2}. Notably, this research not only underscores COF's potential as a high-quality triboelectric material for TENGs but also suggests a strategic approach for chemically designing and creating novel triboelectric layers to build high-efficiency TENGs.

Zhai *et al.* has made significant strides in the development of COFs for use in TENGs.[123] Their study introduced two COFs with similar topologies and frameworks but differing in their charge states, shown in Fig. 9(a). The key innovation lies in the design of a cationic COF, which demonstrates unconventional electrostatic functions owing to the ionic interface within its structure, as shown in Fig. 9(b). The research team designed and synthesized a novel cationic TFP-DB-COF as shown in Fig. 9(c) using 1,3,5-triformylphloroglucinol (TFP) as a neutral knot and dimidium bromide (DB) as a cationic linker through imine condensation. As this COF contrasts with a newly constructed neutral TFP-DP-COF, which lacks ionic groups and uses TFP as a knot and 3,8-diamino-6-phenylphenanthridine (DP) as linker. Both the synthesis reactions occurred in a

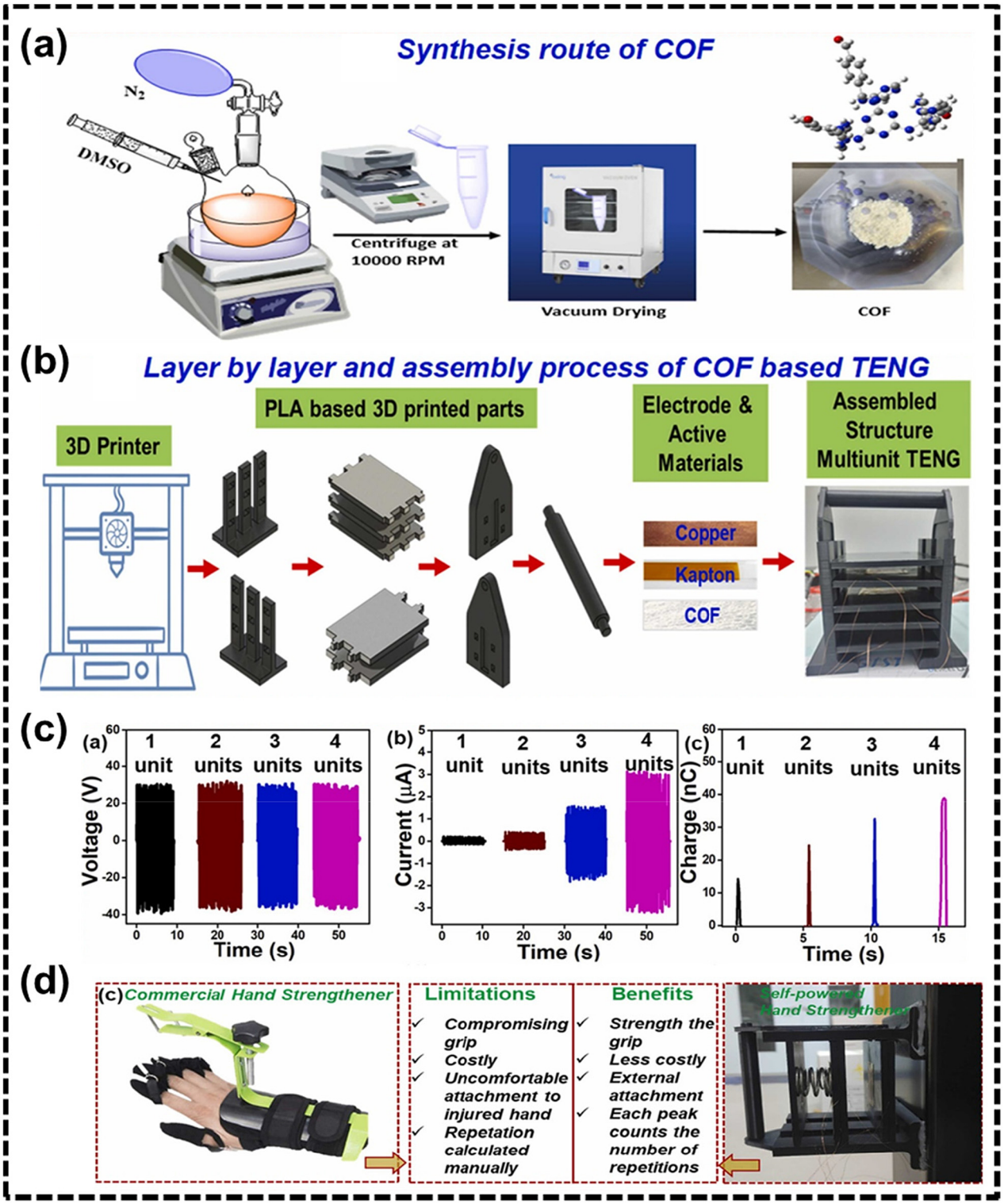

Fig. 8 (a) Synthesis route of COF; (b) layer-by-layer and assembly process of COF-based TENG; and (c) multi-unit TENG voltage, current, charge output of the 4 units of COF-based TENG connected in parallel connection, (d) comparison between commercial system and self-powered hand strengthening device. Reprinted from ref. 17, Copyright © 2022, Elsevier.

mixture solvent of mesitylene and 1,4-dioxane, catalysed by acetic acid, under solvothermal conditions at 120 °C for 3 days. Both TFP-DB-COF and TFP-DP-COF were obtained as red powders, with isolation yields of 76% and 77%, respectively. The physical and chemical properties of both the sample were characterised by FTIR, PXRD, TGA, FESEM-EDX. The presence

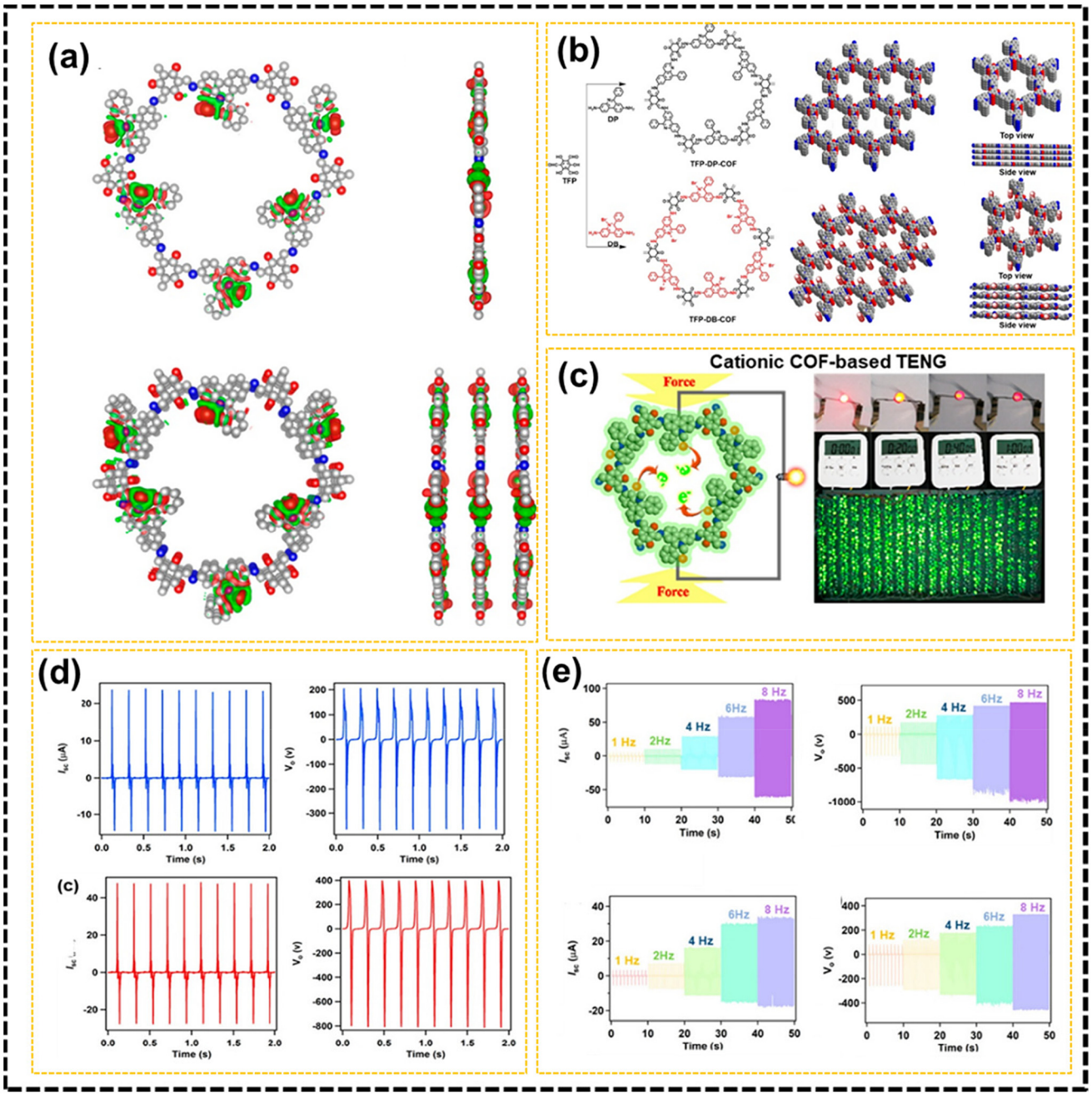

Fig. 9 (a) Charge density difference between TFP-DB-COF and TFP-DP-COF. (b) Schematic representation of the synthesis of TFP-DP-COF and TFP-DB-COF. (c) Photograph of lighting of 1388 LEDs powered by a TFP-DB-COF-based TENG at 8 Hz. (d) I_{sc}, V_0 of TFP-DB-COF and TFP-DP-COF with different working frequencies: 1, 2, 4, 6, and 8 Hz. (e) I_{sc}, V_0 of TFP-DP-COF and TFPDB-COF at 5 Hz. Reprinted from ref. 123, Copyright © 2020, American Chemical Society.

of cationic group was confirmed by CP-MAS ^{13}C solid-state NMR spectroscopy.

The presence of cationic functional centres distributed alternately over both sides of the pore channels in the cationic COF significantly enhances its electrostatic capabilities. Comparative analysis of these COFs in TENG applications reveals a substantial improvement in the output performance of the cationic TFP-DB-COF. When integrated into an electric-dipole-based TENG, the cationic COF exhibits a two-fold increase in performance compared to its neutral counterpart. The output performance was measured under identical mechanical impact conditions, with the cationic COF demonstrating nearly double the short-circuit current and voltage outputs. Specifically, at 5 Hz, the TFP-DB-COF achieved 47.9 μA and 815 V, in contrast to the 23.5 μA and 365 V of the TFP-DP-COF, shown in Fig. 9(d). A TENG device fabricated

using cationic TFP-DB-COF had higher I_{sc} and V_0 as the working frequency increased. Specifically, I_{sc} increased from 5.2 to 82.2 μA and V_0 from 315 to 1000 V. These values exceeded TFP-DP-COF, with I_{sc} values from 2.9 to 34.2 μA and V_0 values from 260 to 460 V due to increasing pushing cycles every unit time and accelerating charge flow rate, as seen in Fig. 9(e). This advancement in COF-based TENG technology not only demonstrates the impact of cationic groups on output performance but also highlights the potential of these devices in practical applications. The cationic COF-based TENG has been successfully used to charge commercial capacitors, illuminate LEDs, and power a stopwatch, showcasing its capability as an eco-friendly and high-performance energy harvesting and self-powered device.[123]

6. Current challenges and future improvements

MOF and COFs facing number of major difficulties that limit their extensive practical use. Both types of materials suffer with stability, especially in harsh environments or under long-term use conditions. Scalability remains a serious challenge, as finding cost-effective, large-scale production processes is critical to industrial adoption.[124,125] MOFs are frequently characterised by limited mechanical strength and electrical conductivity, restricting its usage in specific applications. For COFs, achieving high crystallinity and controlling defects during synthesis are ongoing challenges.[126] Both materials have difficulty processing and integrating into devices while retaining their desirable features. Biocompatibility as well as potential toxicity are issues for biomedical applications.[127] Also, researchers are attempting to enhance the selective functionalization of these materials to alter their characteristics for specific applications. The environmental effect and sustainability of manufacturing processes are increasingly critical factors.[128] Overcoming these challenges is critical for realising MOF and COFs full promise in a variety of disciplines, including catalysis, gas storage, drug delivery, and sensing applications.

Improving electron-withdrawing capabilities will be critical for increasing performance in applications such as triboelectric nanogenerators. For example, including strong electron-drawing groups such as fluorine atoms into MOF structures

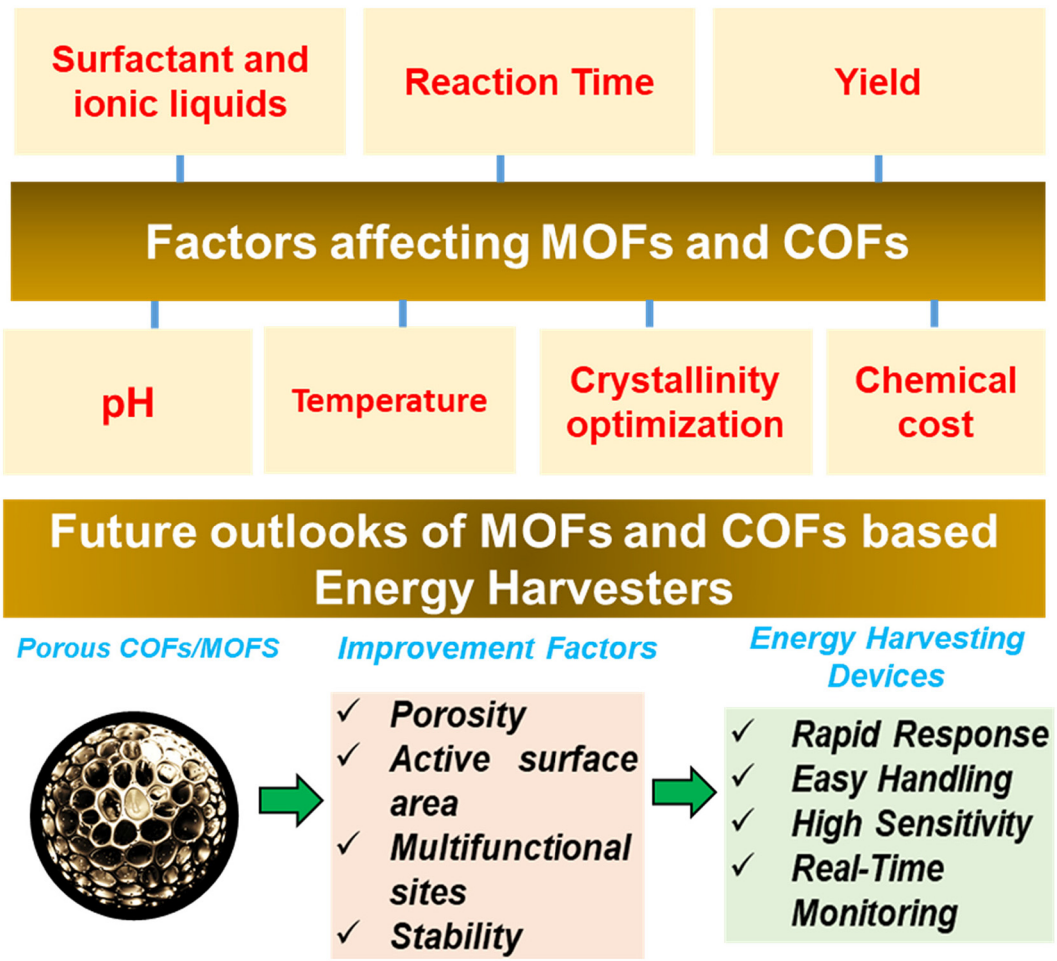

Fig. 10 Overall challenges and possible solutions for framework materials based energy harvesters.

has resulted in notable gains, with the UiO-66-4F MOF exhibiting a 77.5-fold increase in power density over ordinary PDMS triboelectric nanogenerators.[105] Developing more accurate control over structural elements using rational design concepts would enable unprecedented customisation of material properties. This technique based on reticular chemistry allows researchers to design MOF and COFs for specific applications such as catalysis, chemical sensing, water harvesting, gas storage, and separation.[129] Researchers will continue to investigate hybrid structures and composites, such as MOF@COF, COF@MOF, and MOF + COF combinations, to improve performance and widen possible applications. These integrated materials could combine the capabilities of MOFs and COFs, resulting in unique functions.[130,131] Improving the overall stability and endurance of MOFs and COFs is an important subject for future research, especially for practical applications in harsh settings. Scaling up manufacturing processes for industrial application is critical to the broad acceptance of MOFs and COFs. Crystallinity optimisation will most likely require sophisticated techniques such as microwave-assisted synthesis and Bayesian optimisation, both of which can increase the structural integrity and performance of MOFs and COFs. Fig. 10 presents the overall challenges and possible solutions as well as the placement of MOFs and COFs as promising triboelectric materials in the triboelectric series.

6.1 Enhancing stability

Develop MOFs and COFs with higher environmental resilience to withstand harsh conditions and prolonged use, crucial for broader application in real-world environments.

6.2 Scalable production

Research cost-effective, large-scale manufacturing techniques for MOFs and COFs to facilitate industrial adoption, making these frameworks more economically viable for widespread use.

6.3 Improving mechanical strength and conductivity

Increase the mechanical robustness and electrical conductivity of MOFs to broaden their application potential in devices requiring durable, conductive materials.

6.4 Optimizing crystallinity in COFs

Innovate synthesis methods for COFs to achieve high crystallinity and minimize defects, which enhances the structural integrity and consistency of the material properties.

6.5 Efficient integration into devices

Develop advanced processing methods that enable MOFs and COFs to be seamlessly integrated into devices while retaining their beneficial properties.

6.6 Addressing biocompatibility and toxicity

Ensure that MOFs and COFs are biocompatible and non-toxic for safe use in biomedical applications, especially for drug delivery and sensing.

6.7 Reducing environmental impact of synthesis

Emphasize eco-friendly, sustainable manufacturing processes that lower the environmental footprint of MOF and COF production.

6.8 Rational design with reticular Chemistry

Use rational design principles to precisely control structural elements in MOFs and COFs, enabling tailored frameworks optimized for applications such as gas storage, water harvesting, and energy conversion.

7. Conclusions

The review concludes that MOFs and covalent organic frameworks COFs show immense potential for enhancing TENGs. These materials offer unique advantages such as high surface area, tunable structures, and diverse functionalities, making them excellent candidates for triboelectric layers. The successful integration of various MOFs and COFs into TENGs has resulted in improved electrical outputs and energy harvesting capabilities, as demonstrated by examples like ZIF-67 based S-TENGs, fluorinated Tp-TFAB COF TENGs, and cationic COF TENGs. Practical applications of these MOF/COF-based TENGs include powering wristwatches, aiding in object recognition for robotic grippers, and creating self-powered gas sensors. These advancements not only showcase the potential of MOFs and COFs in energy harvesting but also pave the way for sustainable energy technologies and open new possibilities in the field of self-powered devices.

Data availability

Our manuscript does not contain any new experimental data, graphs, or figures. All documents used to support our vision are listed as references with the appropriate links to the original journals.

Conflicts of interest

The authors declare no conflict of interest.

Acknowledgements

This study is supported by the National Research Foundation of Korea (NRF), funded by the Ministry of Science and ICT of Korea (RS-2024-00346135 and RS-2024-00406674). V. V. thank Department of Science and Technology India for the support through PURSE Scheme (SR/PURSE/2023/196).

References

1 Z. L. Wang and J. Song, *Science*, 2006, **312**, 242–246.

2 S. Panda, S. Hajra, K. Mistewicz, P. In-na, M. Sahu, P. M. Rajaitha and H. J. Kim, *Nano Energy*, 2022, **100**, 107514.
3 J. Lee, S. Hajra, S. Panda, W. Oh, Y. Oh, H. Shin, Y. K. Mishra and H. J. Kim, *Int. J. Precis. Eng. Manuf.-Green Technol.*, 2024, **11**, 233–241.
4 S. Panda, S. Hajra, H. Jeong, B. K. Panigrahi, P. Pakawanit, D. Dubal, S. Hong and H. J. Kim, *Nano Energy*, 2022, **102**, 107682.
5 S. Hajra, M. Sahu, D. Oh and H. J. Kim, *Ceram. Int.*, 2021, **47**, 15695–15702.
6 L. Lin, Y. Xie, S. Niu, S. Wang, P.-K. Yang and Z. L. Wang, *ACS Nano*, 2015, **9**, 922–930.
7 M. Rakshita, N. Madathil, A. A. Sharma, P. P. Pradhan, A. K. Kasireddi Durga Prasad, U. K. Khanapuram, R. K. Rajaboina and H. Divi, *ACS Appl. Electron. Mater.*, 2024, **6**, 1821–1828.
8 K. Ruthvik, A. Babu, P. Supraja, M. Navaneeth, V. Mahesh, K. U. Kumar, R. R. Kumar, B. M. Rao, D. Haranath and K. Prakash, *Mater. Lett.*, 2023, **350**, 134947.
9 N. Kumar, B. Mahale, T. S. Muzata and R. Ranjan, *Int. J. Energy Res.*, 2021, **45**, 19395–19404.
10 S. Hajra, A. Ali, S. Panda, H. Song, P. M. Rajaitha, D. Dubal, A. Borras, P. In-Na, N. Vittayakorn, V. Vivekananthan, H. J. Kim, S. Divya and T. H. Oh, *Adv. Energy Mater.*, 2024, **14**, 2400025.
11 X. Zhou, H. Jin, B. Y. Xia, K. Davey, Y. Zheng and S. Z. Qiao, *Adv. Mater.*, 2021, **33**, 2104341.
12 S. Kitagawa, *Chem. Soc. Rev.*, 2014, **43**, 5415–5418.
13 O. M. Yaghi, M. J. Kalmutzki and C. S. Diercks, *Introduction to reticular chemistry: metal-organic frameworks and covalent organic frameworks*, John Wiley & Sons, 2019.
14 R. Freund, O. Zaremba, G. Arnauts, R. Ameloot, G. Skorupskii, M. Dincă, A. Bavykina, J. Gascon, A. Ejsmont and J. Goscianska, *Angew. Chem., Int. Ed.*, 2021, **60**, 23975–24001.
15 O. Yaghi and H. Li, *J. Am. Chem. Soc.*, 1995, **117**, 10401–10402.
16 A. Babu, K. Ruthvik, P. Supraja, M. Navaneeth, K. U. Kumar, R. R. Kumar, K. Prakash and N. Raju, *J. Mater. Sci.: Mater. Electron.*, 2023, **34**, 2195.
17 S. Hajra, J. Panda, J. Swain, H.-G. Kim, M. Sahu, M. K. Rana, R. Samantaray, H. J. Kim and R. Sahu, *Nano Energy*, 2022, **101**, 107620.
18 A. P. Cote, A. I. Benin, N. W. Ockwig, M. O'Keeffe, A. J. Matzger and O. M. Yaghi, *science*, 2005, **310**, 1166–1170.
19 X. Cui, H. Dong, S. Chen, M. Wu and Y. Wang, *Batteries Supercaps*, 2021, **4**, 72–97.
20 Y. Bai, C. Liu, Y. Shan, T. Chen, Y. Zhao, C. Yu and H. Pang, *Adv. Energy Mater.*, 2022, **12**, 2100346.
21 W. Li, X. Zhao, Q. Bi, Q. Ma, L. Han and K. Tao, *Dalton Trans.*, 2021, **50**, 11701–11710.
22 H. Peng, J. Raya, F. Richard, W. Baaziz, O. Ersen, A. Ciesielski and P. Samorì, *Angew. Chem., Int. Ed.*, 2020, **59**, 19602–19609.
23 N. An, Z. Guo, J. Xin, Y. He, K. Xie, D. Sun, X. Dong and Z. Hu, *J. Mater. Chem. A*, 2021, **9**, 16824–16833.
24 S. Kandambeth, J. Jia, H. Wu, V. S. Kale, P. T. Parvatkar, J. Czaban-Jóźwiak, S. Zhou, X. Xu, Z. O. Ameur and E. Abou-Hamad, *Adv. Energy Mater.*, 2020, **10**, 2001673.
25 M. Wang, H. Guo, R. Xue, Q. Li, H. Liu, N. Wu, W. Yao and W. Yang, *ChemElectroChem*, 2019, **6**, 2984–2997.
26 Y. Yang, P. Zhang, L. Hao, P. Cheng, Y. Chen and Z. Zhang, *Angew. Chem., Int. Ed.*, 2021, **60**, 21838–21845.
27 C. R. DeBlase, K. E. Silberstein, T.-T. Truong, H. D. Abruña and W. R. Dichtel, *J. Am. Chem. Soc.*, 2013, **135**, 16821–16824.
28 Z. Yang, J. Liu, Y. Li, G. Zhang, G. Xing and L. Chen, *Angew. Chem.*, 2021, **133**, 20922–20927.
29 C. Montoro, D. Rodríguez-San-Miguel, E. Polo, R. Escudero-Cid, M. L. Ruiz-González, J. A. Navarro, P. Ocón and F. Zamora, *J. Am. Chem. Soc.*, 2017, **139**, 10079–10086.
30 Y. Yang, X. He, P. Zhang, Y. H. Andaloussi, H. Zhang, Z. Jiang, Y. Chen, S. Ma, P. Cheng and Z. Zhang, *Angew. Chem.*, 2020, **132**, 3707–3713.
31 D. W. Kang, M. Kang and C. S. Hong, *J. Mater. Chem. A*, 2020, **8**, 7474–7494.
32 I. A. Khan, Y. Qian, A. Badshah, M. A. Nadeem and D. Zhao, *ACS Appl. Mater. Interfaces*, 2016, **8**, 17268–17275.
33 L. Kong, M. Zhong, W. Shuang, Y. Xu and X.-H. Bu, *Chem. Soc. Rev.*, 2020, **49**, 2378–2407.
34 D. Li, T. Liu, Z. Yan, L. Zhen, J. Liu, J. Wu and Y. Feng, *ACS Appl. Mater. Interfaces*, 2020, **12**, 7030–7037.
35 R. K. Tripathy, A. K. Samantara and J. Behera, *Sustainable Energy Fuels*, 2021, **5**, 1184–1193.
36 P. Horcajada, T. Chalati, C. Serre, B. Gillet, C. Sebrie, T. Baati, J. F. Eubank, D. Heurtaux, P. Clayette and C. Kreuz, *Nat. Mater.*, 2010, **9**, 172–178.
37 K. Suresh and A. J. Matzger, *Angew. Chem., Int. Ed.*, 2019, **58**, 16790–16794.
38 T. Huo, Y. Yang, M. Qian, H. Jiang, Y. Du, X. Zhang, Y. Xie and R. Huang, *Biomaterials*, 2020, **260**, 120305.
39 L. Ge, C. Qiao, Y. Tang, X. Zhang and X. Jiang, *Nano Lett.*, 2021, **21**, 3218–3224.
40 H. Singh, V. K. Tomer, N. Jena, I. Bala, N. Sharma, D. Nepak, A. De Sarkar, K. Kailasam and S. K. Pal, *J. Mater. Chem. A*, 2017, **5**, 21820–21827.
41 M. Liu, Y. J. Chen, X. Huang, L. Z. Dong, M. Lu, C. Guo, D. Yuan, Y. Chen, G. Xu and S. L. Li, *Angew. Chem., Int. Ed.*, 2022, **61**, e202115308.
42 Y. Lu, W. Zhan, Y. He, Y. Wang, X. Kong, Q. Kuang, Z. Xie and L. Zheng, *ACS Appl. Mater. Interfaces*, 2014, **6**, 4186–4195.
43 Y. Cao, L. Wang, C. Shen, C. Wang, X. Hu and G. Wang, *Sens. Actuators, B*, 2019, **283**, 487–494.
44 Y. Li and R. T. Yang, *Langmuir*, 2007, **23**, 12937–12944.
45 T. G. Glover, G. W. Peterson, B. J. Schindler, D. Britt and O. Yaghi, *Chem. Eng. Sci.*, 2011, **66**, 163–170.
46 P. Das and S. K. Mandal, *Chem. Mater.*, 2019, **31**, 1584–1596.

47 H. Furukawa and O. M. Yaghi, *J. Am. Chem. Soc.*, 2009, **131**, 8875–8883.
48 Y. Ying, S. B. Peh, H. Yang, Z. Yang and D. Zhao, *Adv. Mater.*, 2022, **34**, 2104946.
49 H. Fan, A. Mundstock, A. Feldhoff, A. Knebel, J. Gu, H. Meng and J. r. Caro, *J. Am. Chem. Soc.*, 2018, **140**, 10094–10098.
50 Y. Wang, H. Jin, Q. Ma, K. Mo, H. Mao, A. Feldhoff, X. Cao, Y. Li, F. Pan and Z. Jiang, *Angew. Chem.*, 2020, **132**, 4395–4399.
51 Y.-Z. Li, G.-D. Wang, L.-N. Ma, L. Hou, Y.-Y. Wang and Z. Zhu, *ACS Appl. Mater. Interfaces*, 2021, **13**, 4102–4109.
52 P. García-García, M. Müller and A. Corma, *Chem. Sci.*, 2014, **5**, 2979–3007.
53 X. Wang, X. Han, J. Zhang, X. Wu, Y. Liu and Y. Cui, *J. Am. Chem. Soc.*, 2016, **138**, 12332–12335.
54 S. Daliran, A. R. Oveisi, Y. Peng, A. López-Magano, M. Khajeh, R. Mas-Ballesté, J. Alemán, R. Luque and H. Garcia, *Chem. Soc. Rev.*, 2022, **51**, 7810–7882.
55 S. S. Han, H. Furukawa, O. M. Yaghi and W. A. Goddard III, *J. Am. Chem. Soc.*, 2008, **130**, 11580–11581.
56 S. J. Yang, T. Kim, J. H. Im, Y. S. Kim, K. Lee, H. Jung and C. R. Park, *Chem. Mater.*, 2012, **24**, 464–470.
57 J. Ren, N. M. Musyoka, H. W. Langmi, A. Swartbooi, B. C. North and M. Mathe, *Int. J. Hydrogen Energy*, 2015, **40**, 4617–4622.
58 S. Hajra, M. Sahu, A. M. Padhan, I. S. Lee, D. K. Yi, P. Alagarsamy, S. S. Nanda and H. J. Kim, *Adv. Funct. Mater.*, 2021, **31**, 2101829.
59 R. A. Shaukat, Q. M. Saqib, J. Kim, H. Song, M. U. Khan, M. Y. Chougale, J. Bae and M. J. Choi, *Nano Energy*, 2022, **96**, 107128.
60 O. M. Yaghi, M. O'Keeffe, N. W. Ockwig, H. K. Chae, M. Eddaoudi and J. Kim, *Nature*, 2003, **423**, 705–714.
61 V. Kumar, P. Kumar, R. Deka, Z. Abbas and S. M. Mobin, *Chem. Rec.*, 2022, **22**, e202200067.
62 L. Chen, R. Luque and Y. Li, *Chem. Soc. Rev.*, 2017, **46**, 4614–4630.
63 M. Ding, X. Cai and H.-L. Jiang, *Chem. Sci.*, 2019, **10**, 10209–10230.
64 X. Zhang, Z. Chen, X. Liu, S. L. Hanna, X. Wang, R. Taheri-Ledari, A. Maleki, P. Li and O. K. Farha, *Chem. Soc. Rev.*, 2020, **49**, 7406–7427.
65 H. Furukawa, K. E. Cordova, M. O'Keeffe and O. M. Yaghi, *Science*, 2013, **341**, 1230444.
66 G. M. Whitesides, E. E. Simanek, J. P. Mathias, C. T. Seto, D. Chin, M. Mammen and D. M. Gordon, *Acc. Chem. Res.*, 1995, **28**, 37–44.
67 L. Zang, Y. Che and J. S. Moore, *Acc. Chem. Res.*, 2008, **41**, 1596–1608.
68 M. O'Keeffe, *Chem. Soc. Rev.*, 2009, **38**, 1215–1217.
69 M. O'Keeffe and O. M. Yaghi, *Chem. Rev.*, 2012, **112**, 675–702.
70 M. Eddaoudi, D. B. Moler, H. Li, B. Chen, T. M. Reineke, M. O'keeffe and O. M. Yaghi, *Acc. Chem. Res.*, 2001, **34**, 319–330.
71 Y. Zheng, F. Z. Sun, X. Han, J. Xu and X. H. Bu, *Adv. Opt. Mater.*, 2020, **8**, 2000110.
72 Z. Jiang, P. Zhou, T. Xu, L. Fan, S. Hu, J. Chen and Y. He, *CrystEngComm*, 2020, **22**, 3424–3431.
73 F. A. A. Paz, J. Klinowski, S. M. Vilela, J. P. Tome, J. A. Cavaleiro and J. Rocha, *Chem. Soc. Rev.*, 2012, **41**, 1088–1110.
74 K. S. Park, Z. Ni, A. P. Côté, J. Y. Choi, R. Huang, F. J. Uribe-Romo, H. K. Chae, M. O'Keeffe and O. M. Yaghi, *Proc. Natl. Acad. Sci. U. S. A.*, 2006, **103**, 10186–10191.
75 N. Stock and S. Biswas, *Chem. Rev.*, 2012, **112**, 933–969.
76 R. Banerjee, A. Phan, B. Wang, C. Knobler, H. Furukawa, M. O'Keeffe and O. M. Yaghi, *Science*, 2008, **319**, 939–943.
77 D. Zou, S. P. Nunes, I. F. Vankelecom, A. Figoli and Y. M. Lee, *Green Chem.*, 2021, **23**, 9815–9843.
78 J. Swain, A. Priyadarshini, S. Hajra, S. Panda, J. Panda, R. Samantaray, Y. Yamauchi, M. Han, H. J. Kim and R. Sahu, *J. Alloys Compd.*, 2023, **965**, 171438.
79 J. Panda, S. Soren, J. Swain, A. Priyadarshini, S. Swain, R. Sahu and R. Samantaray, *AIP Conf. Proc.*, 2023, **2740**, 040006.
80 J. Panda, S. P. Biswal, H. S. Jena, A. Mitra, R. Samantray and R. Sahu, *Catalysts*, 2022, **12**, 494.
81 J. Panda, J. K. Sahoo, P. K. Panda, S. N. Sahu, M. Samal, S. K. Pattanayak and R. Sahu, *J. Mol. Liq.*, 2019, **278**, 536–545.
82 J. M. Gonçalves, B. N. Safadi, B. A. Iglesias, P. R. Martins, L. Angnes and K. Araki, *Supramolecular Nanotechnology: Advanced Design of Self-Assembled Functional Materials*, 2023, vol. 1, pp. 123–150.
83 S. Barsiwal, A. Babu, U. K. Khanapuram, S. Potu, N. Madathil, R. K. Rajaboina, S. Mishra, H. Divi, P. Kodali and R. Nagapuri, *Nanoenergy Adv.*, 2022, **2**, 291–302.
84 J. Fan, M. Yuan, L. Wang, Q. Xia, H. Zheng and A. Zhou, *Nano Energy*, 2023, **105**, 107973.
85 F. Zhang, Y. Qian, Z. Jin, Z. Fei, J. Zhang, H. Mao, D. J. Kang and H. Pang, *J. Energy Storage*, 2023, **72**, 108213.
86 M. Sundriyal, S. Sundriyal, V. Shrivastav, A. Deep and U. K. Tiwari, *Electrochemical Society Meeting Abstracts 242*, The Electrochemical Society, Inc., 2022, pp. 2417–2417.
87 M. Sánchez-Sánchez, N. Getachew, K. Díaz, M. Díaz-García, Y. Chebude and I. Díaz, *Green Chem.*, 2015, **17**, 1500–1509.
88 S. Hajra, M. Sahu, R. Sahu, A. M. Padhan, P. Alagarsamy, H.-G. Kim, H. Lee, S. Oh, Y. Yamauchi and H. J. Kim, *Nano Energy*, 2022, **98**, 107253.
89 B. Diaz de Grenu, J. Torres, J. García-González, S. Muñoz-Pina, R. de Los Reyes, A. M. Costero, P. Amorós and J. V. Ros-Lis, *ChemSusChem*, 2021, **14**, 208–233.
90 S. Gaikwad and S. Han, *Green Chemical Synthesis with Microwaves and Ultrasound*, 2024, pp. 249–282.
91 S. Głowniak, B. Szczęśniak, J. Choma and M. Jaroniec, *Molecules*, 2023, **28**, 2639.

92 Y. Liu, Y. Wei, M. Liu, Y. Bai, X. Wang, S. Shang, J. Chen and Y. Liu, *Angew. Chem., Int. Ed.*, 2021, **60**, 2887–2891.
93 H. Ren and T. Wei, *ChemElectroChem*, 2022, **9**, e202200196.
94 M. Bechelany, M. Drobek, C. Vallicari, A. A. Chaaya, A. Julbe and P. Miele, *Nanoscale*, 2015, **7**, 5794–5802.
95 Y. Dou, W. Zhang and A. Kaiser, *Adv. Sci.*, 2020, **7**, 1902590.
96 G. W. Peterson, D. T. Lee, H. F. Barton, T. H. Epps III and G. N. Parsons, *Nat. Rev. Mater.*, 2021, **6**, 605–621.
97 M. Rose, B. Böhringer, M. Jolly, R. Fischer and S. Kaskel, *Adv. Eng. Mater.*, 2011, **13**, 356–360.
98 B. Mohan, R. Kumari, Virender, G. Singh, K. Singh, A. J. L. Pombeiro, X. Yang and P. Ren, *Environ. Int.*, 2023, **175**, 107928.
99 D.-G. Wang, T. Qiu, W. Guo, Z. Liang, H. Tabassum, D. Xia and R. Zou, *Energy Environ. Sci.*, 2021, **14**, 688–728.
100 Y. Zhao, Z. Song, X. Li, Q. Sun, N. Cheng, S. Lawes and X. Sun, *Energy Storage Mater.*, 2016, **2**, 35–62.
101 J. Shao, T. Jiang and Z. Wang, *Sci. China: Technol. Sci.*, 2020, **63**, 1087–1109.
102 B.-Y. Lee, D. H. Kim, J. Park, K.-I. Park, K. J. Lee and C. K. Jeong, *Sci. Technol. Adv. Mater.*, 2019, **20**, 758–773.
103 Y. Liu, J. Mo, Q. Fu, Y. Lu, N. Zhang, S. Wang and S. Nie, *Adv. Funct. Mater.*, 2020, **30**, 2004714.
104 Y.-M. Wang, X. Zhang, D. Yang, L. Wu, J. Zhang, T. Lei and R. Yang, *Nanotechnology*, 2022, **33**, 065402.
105 Y.-M. Wang, X. Zhang, C. Liu, L. Wu, J. Zhang, T. Lei, Y. Wang, X.-B. Yin and R. Yang, *Nano Energy*, 2023, **107**, 108149.
106 C. Huang, G. Lu, N. Qin, Z. Shao, D. Zhang, C. Soutis, Y.-Y. Zhang, L. Mi and H. Hou, *ACS Appl. Mater. Interfaces*, 2022, **14**, 16424–16434.
107 G. Khandelwal, N. P. M. J. Raj, V. Vivekananthan and S.-J. Kim, *iScience*, 2021, **24**, 102064.
108 J. Swain, S. Hajra, N. Das, P. Parhi, S. Panda, A. Priyadarshini, J. Panda, A. K. Sahu, P. Alagarsamy and V. Vivekananthan, *Energy Technol.*, 2023, **11**, 2300498.
109 S. Mula, L. Donà, B. Civalleri and M. A. Van Der Veen, *ACS Appl. Mater. Interfaces*, 2022, **14**, 50803–50814.
110 G. Khandelwal, A. Chandrasekhar, N. P. M. J. Raj and S. J. Kim, *Adv. Energy Mater.*, 2019, **9**, 1803581.
111 A. Somov, A. Baranov and D. Spirjakin, *Sens. Actuators, A*, 2014, **210**, 157–164.
112 S.-J. Chen, D. C. Hovde, K. A. Peterson and A. W. Marshall, *Fire Saf. J.*, 2007, **42**, 507–515.
113 H.-Z. Ma, C. Luo, J.-N. Zhao, Y. Shao, Y.-H. Zhang, X. Liu, S. Li, B. Yin, K. Zhang and K. Ke, *ACS Appl. Mater. Interfaces*, 2023, **15**, 37563–37570.
114 S. Hajra, M. Sahu, A. M. Padhan, J. Swain, B. K. Panigrahi, H.-G. Kim, S.-W. Bang, S. Park, R. Sahu and H. J. Kim, *J. Mater. Chem. C*, 2021, **9**, 17319–17330.
115 G. Khandelwal, N. P. M. J. Raj and S.-J. Kim, *J. Mater. Chem. A*, 2020, **8**, 17817–17825.
116 P. K. Nitha and A. Chandrasekhar, *ACS Appl. Electron. Mater.*, 2024, **6**, 5314–5327.
117 S. Sarfudeen, P. K. Nitha, S. A. Basith, M. Varghese, P. Jhariat, A. Chandrasekhar and T. Panda, *ACS Appl. Mater. Interfaces*, 2024, **16**, 24851–24862.
118 S. Barsiwal, A. Babu, U. K. Khanapuram, S. Potu, N. Madathil, R. K. Rajaboina, S. Mishra, H. Divi, P. Kodali, R. Nagapuri and T. Chinthakuntla, *Nanoenergy Adv.*, 2022, **2**, 291–302.
119 M. H. Memon, U.-E.-S. Amjad, A. Mir and M. Mustafa, *ACS Appl. Electron. Mater.*, 2024, **6**, 2178–2187.
120 Z. Abbas, A. P. S. Prasanna, M. Anithkumar, T. S. Bincy, N. Hussain, S.-J. Kim and S. M. Mobin, *Nano Energy*, 2024, **132**, 110344.
121 Z. Abbas, M. Anithkumar, A. P. S. Prasanna, N. Hussain, S.-J. Kim and S. M. Mobin, *J. Mater. Chem. A*, 2023, **11**, 26531–26542.
122 L. Shi, V. S. Kale, Z. Tian, X. Xu, Y. Lei, S. Kandambeth, Y. Wang, P. T. Parvatkar, O. Shekhah and M. Eddaoudi, *Adv. Funct. Mater.*, 2023, **33**, 2212891.
123 L. Zhai, W. Wei, B. Ma, W. Ye, J. Wang, W. Chen, X. Yang, S. Cui, Z. Wu and C. Soutis, *ACS Mater. Lett.*, 2020, **2**, 1691–1697.
124 B. I. Ahmad, K. T. Keasler, E. E. Stacy, S. Meng, T. J. Hicks and P. J. Milner, *Chem. Mater.*, 2023, **35**, 4883–4896.
125 C. H. Hendon, A. J. Rieth, M. D. Korzynski and M. Dinca, *ACS Cent. Sci.*, 2017, **3**, 554–563.
126 P. Kumar, E. Vejerano, A. Khan, G. Lisak, J. H. Ahn and K.-H. Kim, *Korean J. Chem. Eng.*, 2019, **36**, 1839–1853.
127 A. Wang, M. Walden, R. Ettlinger, F. Kiessling, J. J. Gassensmith, T. Lammers, S. Wuttke and Q. Peña, *Adv. Funct. Mater.*, 2023, 2308589.
128 X. Zhang, S. Zhang, Y. Tang, X. Huang and H. Pang, *Composites, Part B*, 2022, **230**, 109532.
129 X. Han, W. Zhang, Z. Chen, Y. Liu and Y. Cui, *Mater. Horiz.*, 2023, **10**, 5337–5342.
130 X. Li, S. Cai, B. Sun, C. Yang, J. Zhang and Y. Liu, *Matter*, 2020, **3**, 1507–1540.
131 R. K. Rajaboina, U. K. Khanapuram, V. Vivekananthan, G. Khandelwal, S. Potu, A. Babu, N. Madathil, M. Velpula and P. Kodali, *Small*, 2024, **20**, 2306209.